Chapter-IV

Results and Discussion

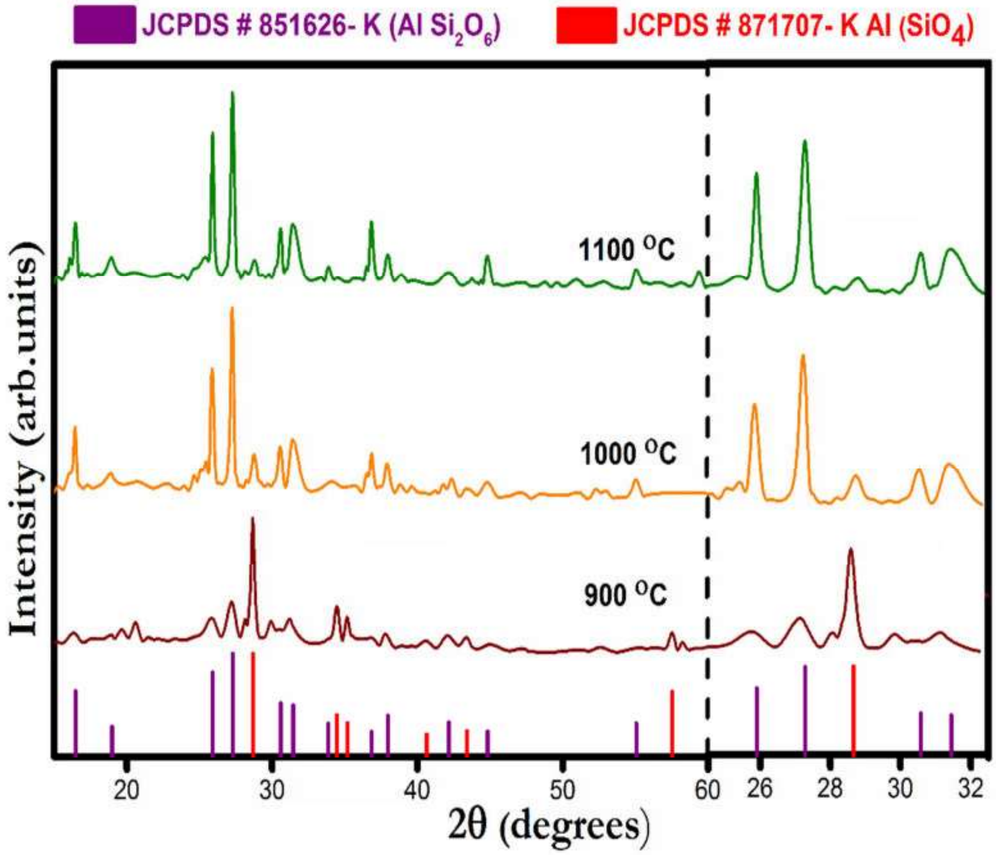

[redacted]

[redacted]

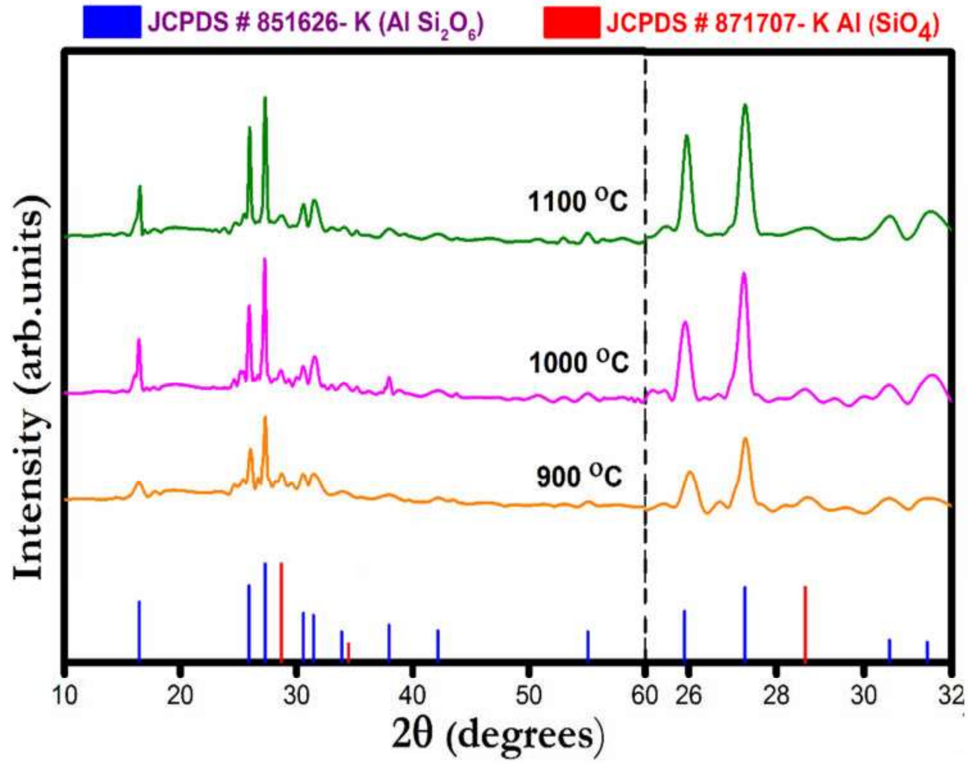

JCPDS # 851626- K (Al Si2O6)
JCPDS # 871707- K Al (SiO4)
1100 °C
1000 °C
900 °C
Intensity (arb.units)
10
20
30
40
50
60
26
28
30
32
2θ (degrees)

[redacted]

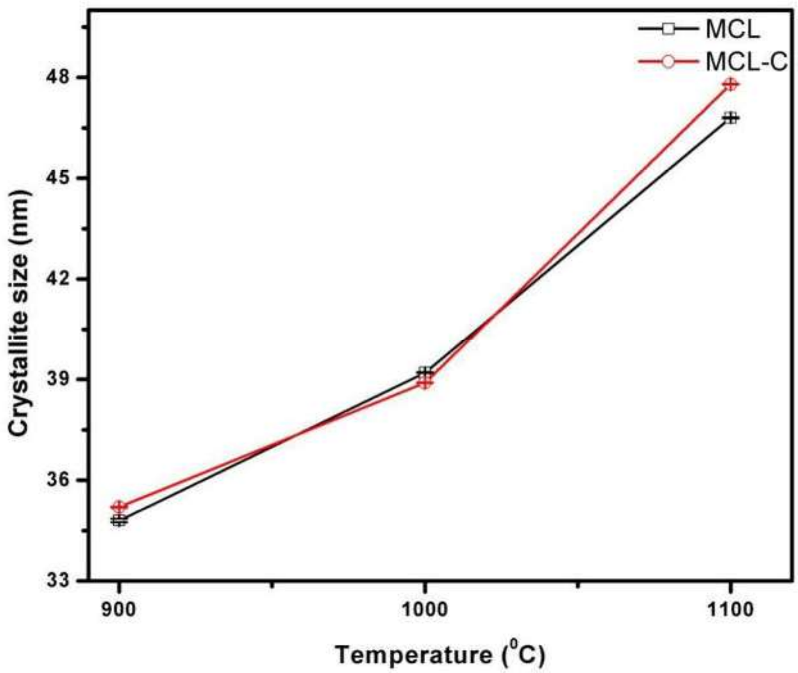

[redacted]

[redacted]

[redacted]

[redacted] g [redacted]

[redacted]

[redacted]	[redacted]	[redacted]	[redacted]
1000	-6 [redacted]	[redacted]	[redacted]
1100	-6 [redacted]	[redacted]	[redacted]
1000	-6 [redacted]	[redacted]	[redacted]
1100	-6 [redacted]	[redacted]	[redacted]

[redacted] 6 [redacted] 6 [redacted] 6 [redacted] g [redacted]

-6 [redacted]

[redacted]

1100 2 [redacted]

[redacted]

[redacted]

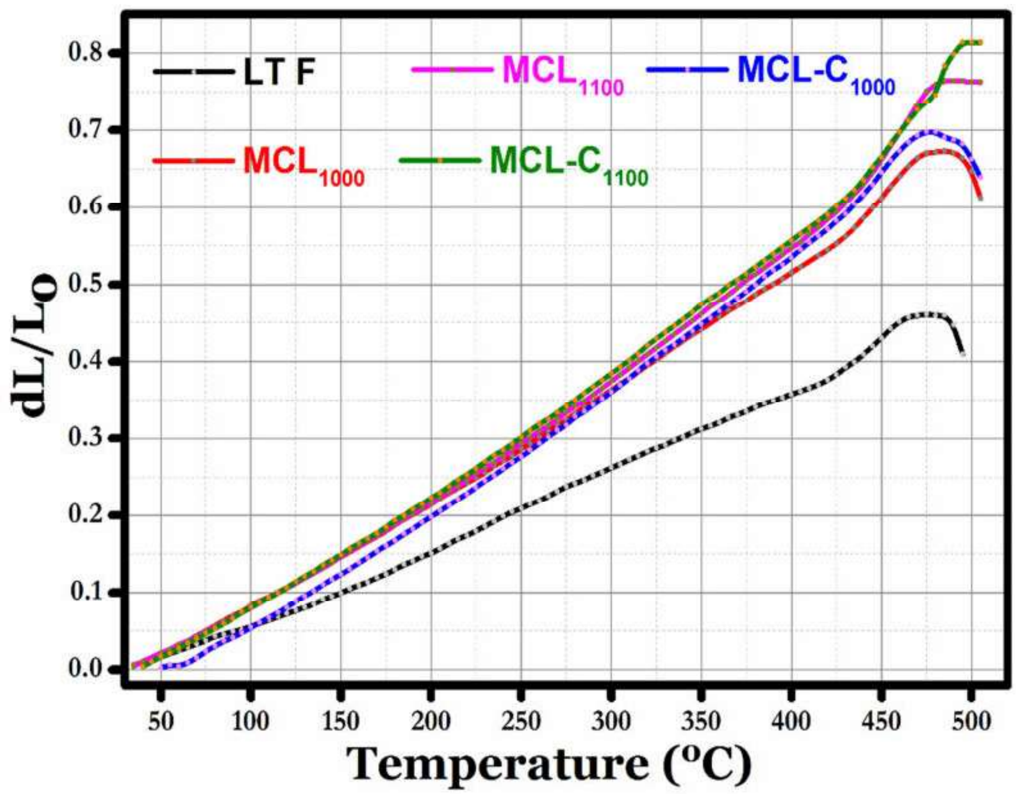

[redacted]

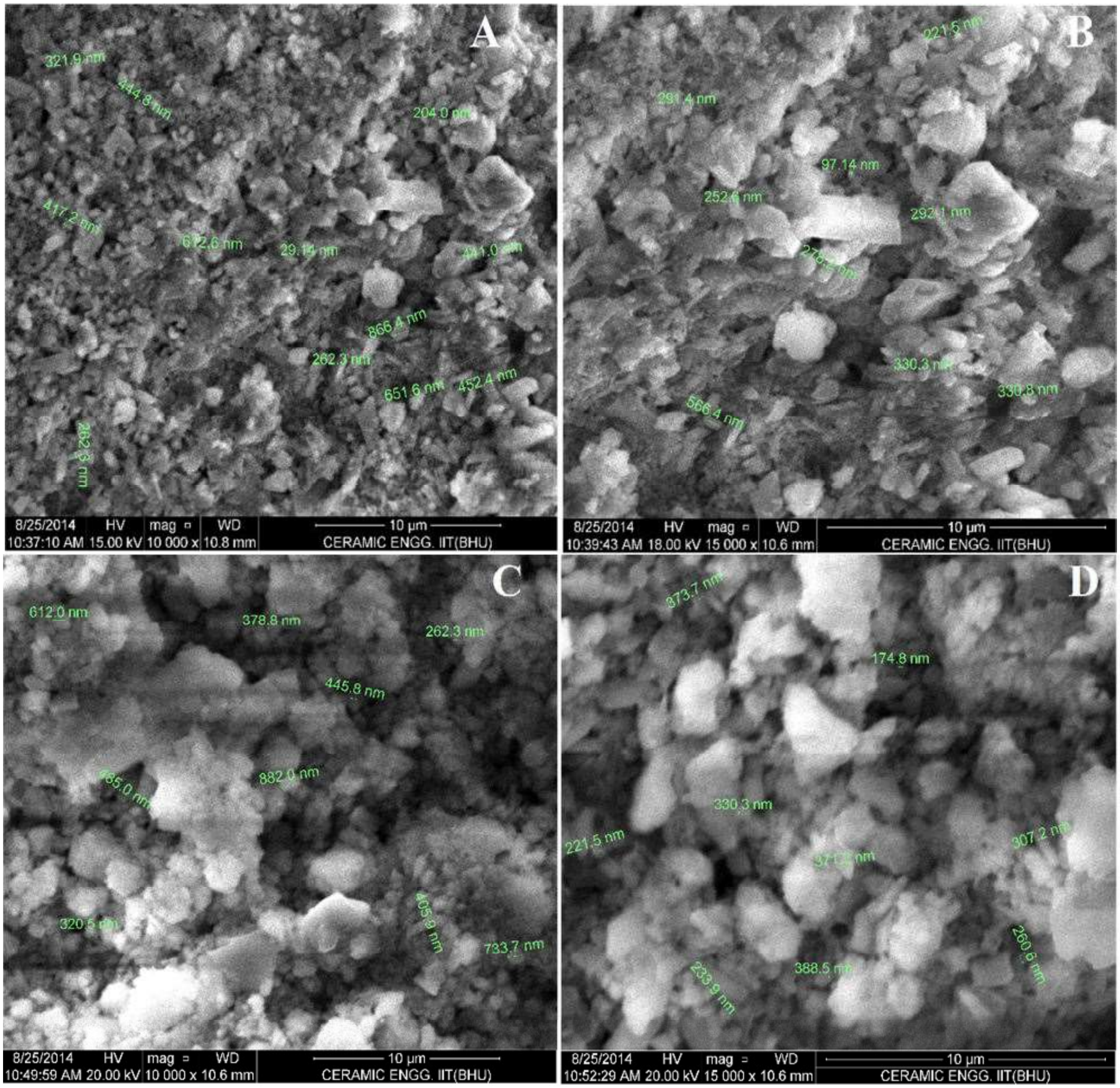
A
B
C
D
8/25/2014 HV mag WD 10 µm
10:37:10 AM 15.00 kV 10 000 x 10.8 mm CERAMIC ENGG. IIT(BHU)
8/25/2014 HV mag WD 10 µm
10:39:43 AM 18.00 kV 15 000 x 10.6 mm CERAMIC ENGG. IIT(BHU)
8/25/2014 HV mag WD 10 µm
10:49:59 AM 20.00 kV 10 000 x 10.6 mm CERAMIC ENGG. IIT(BHU)
8/25/2014 HV mag WD 10 µm
10:52:29 AM 20.00 kV 15 000 x 10.6 mm CERAMIC ENGG. IIT(BHU)

1100

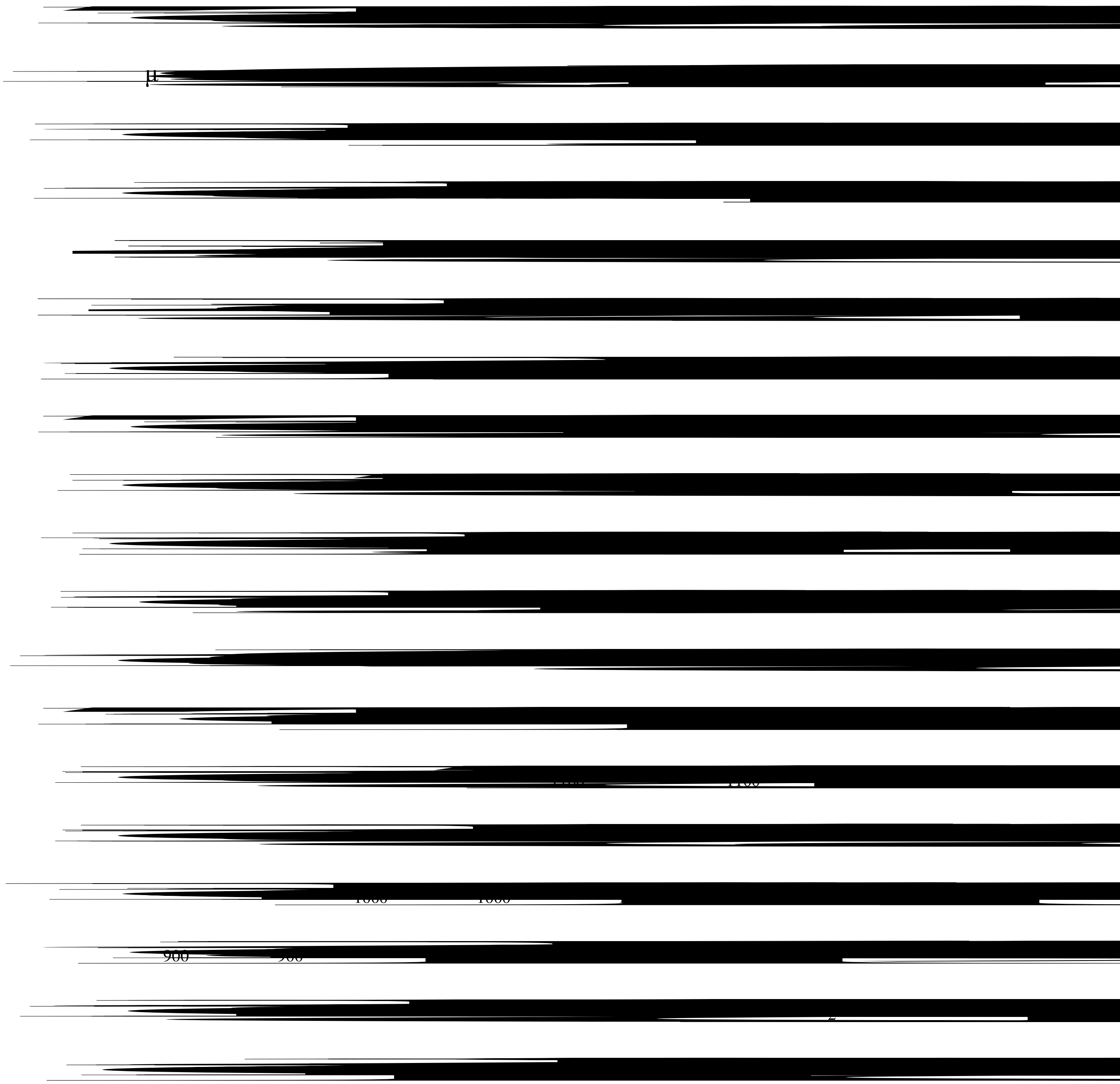

[redacted]

				σ_0	2
1000	[redacted]				
1100	[redacted]				
1000	[redacted]				
1100	[redacted]				

*SD-Standard Deviation; m-Weibull modulus; σ_0-Characteristic strength;

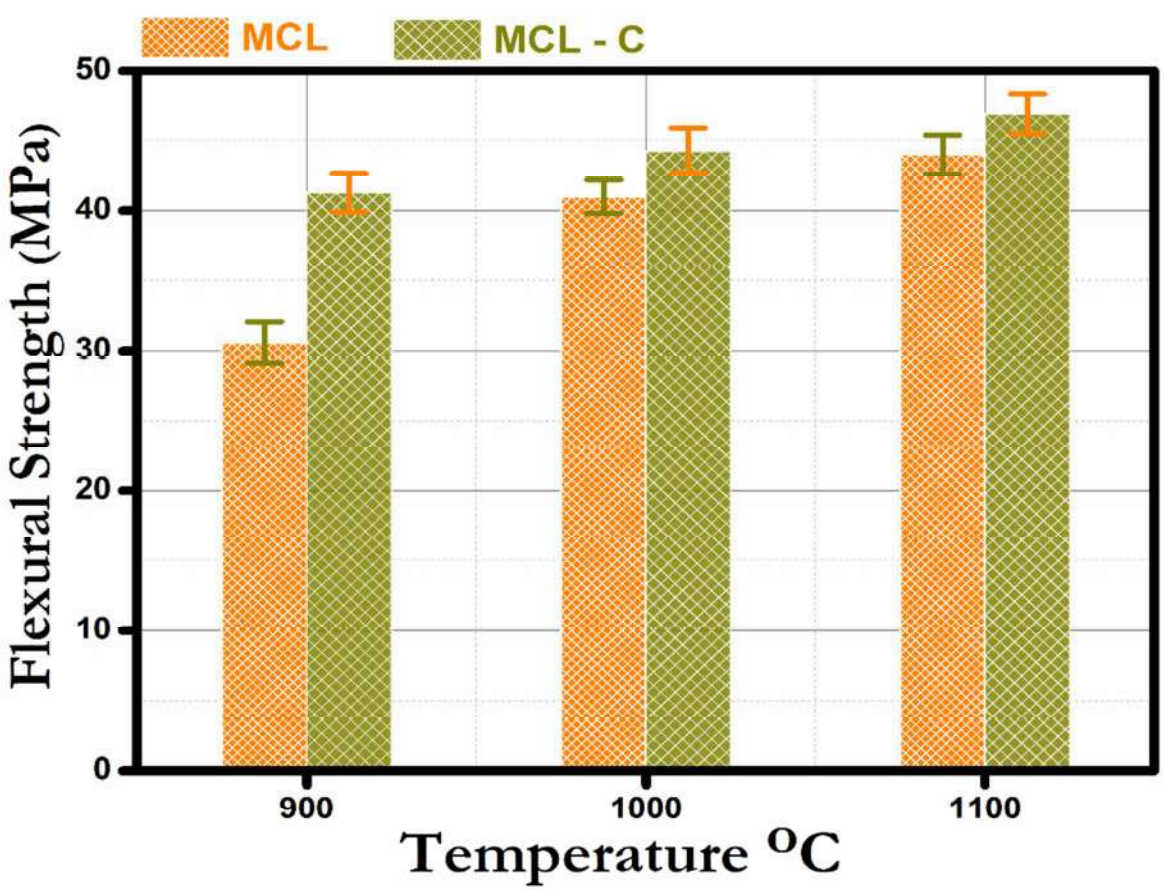

[redacted]

900

1100

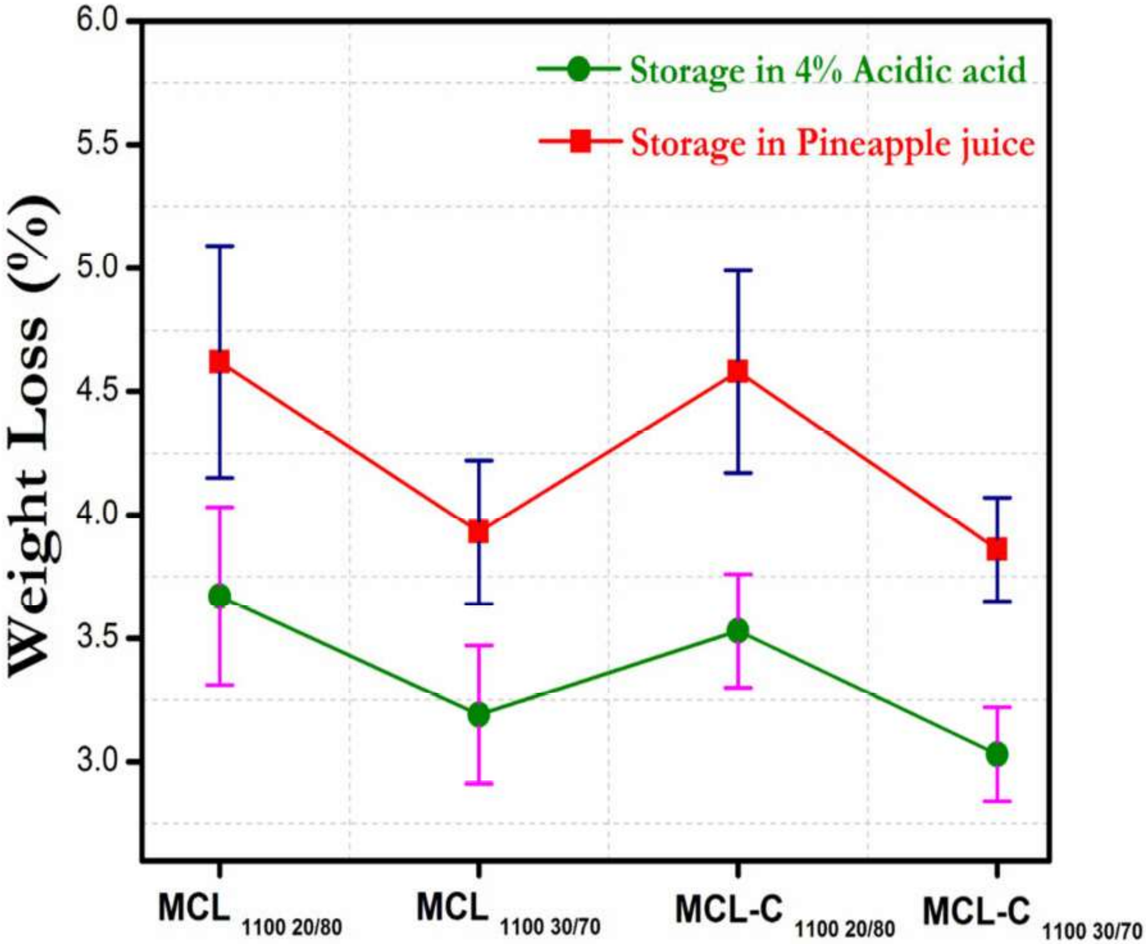

Storage in 4% Acidic acid
Storage in Pineapple juice
Weight Loss (%)
6.0
5.5
5.0
4.5
4.0
3.5
3.0
MCL 1100 20/80
MCL 1100 30/70
MCL-C 1100 20/80
MCL-C 1100 30/70

[illegible]	[illegible]	[illegible]	[illegible]	[illegible]	[illegible]
$MCL_{20/80}$	[illegible]	[illegible]	[illegible]	[illegible]	[illegible]
$MCL_{30/70}$	[illegible]	[illegible]	[illegible]	[illegible]	[illegible]
$MCL\text{-}C_{20/80}$	[illegible]	[illegible]	[illegible]	[illegible]	[illegible]
$MCL\text{-}C_{30/70}$	[illegible]	[illegible]	[illegible]	[illegible]	[illegible]

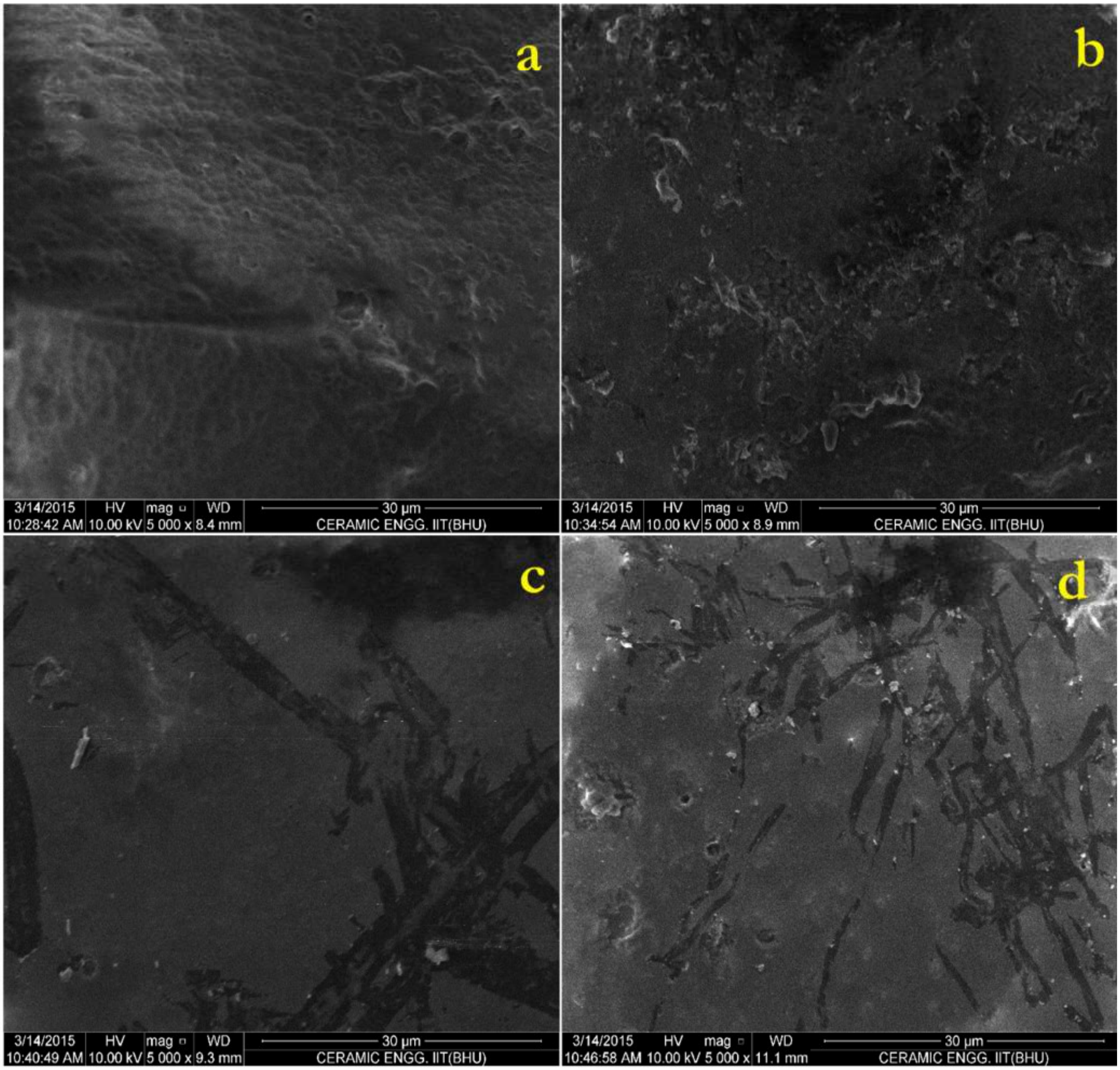

20/80 30/70 20/80

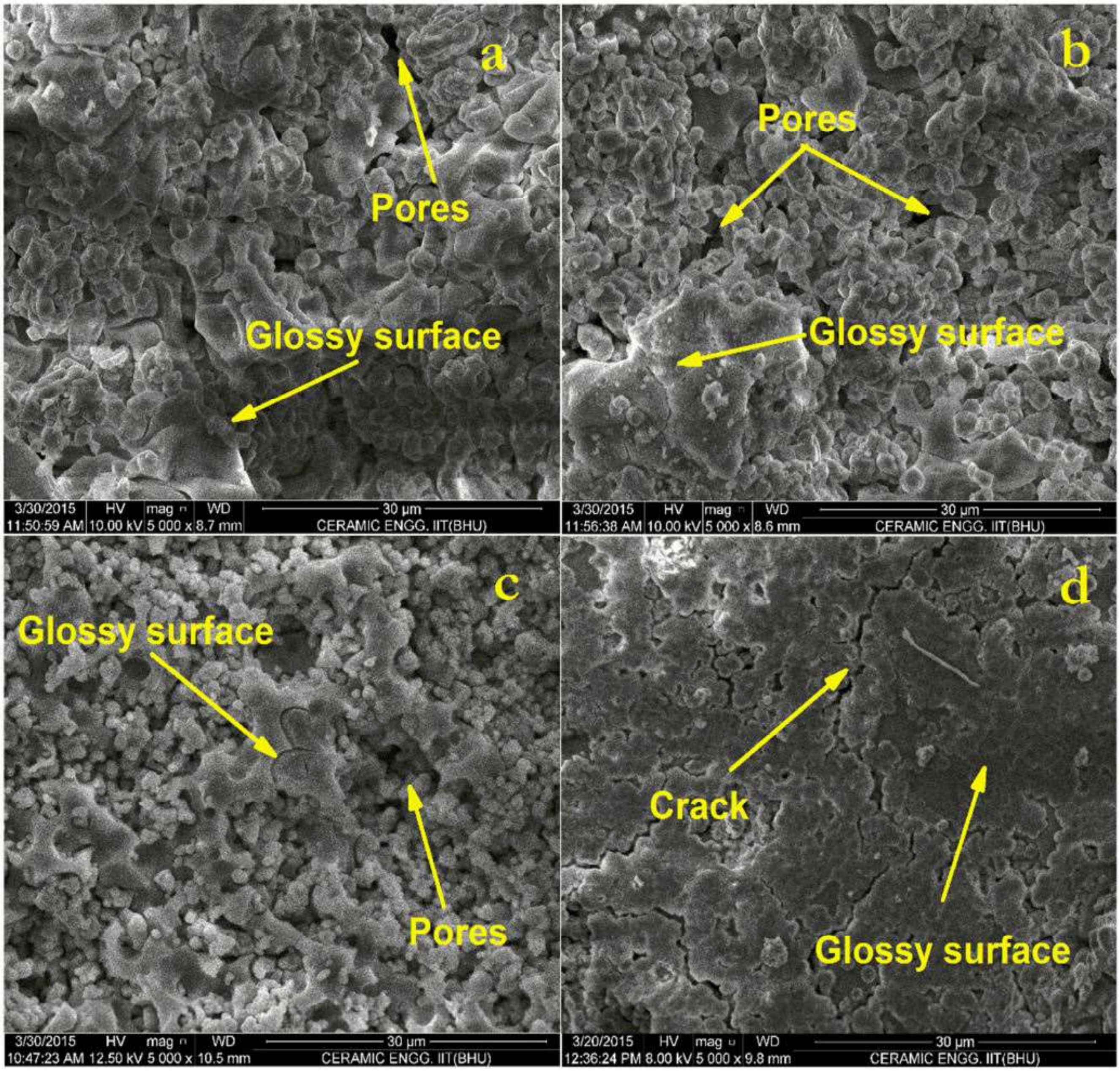

[redacted]

30/70 [redacted]

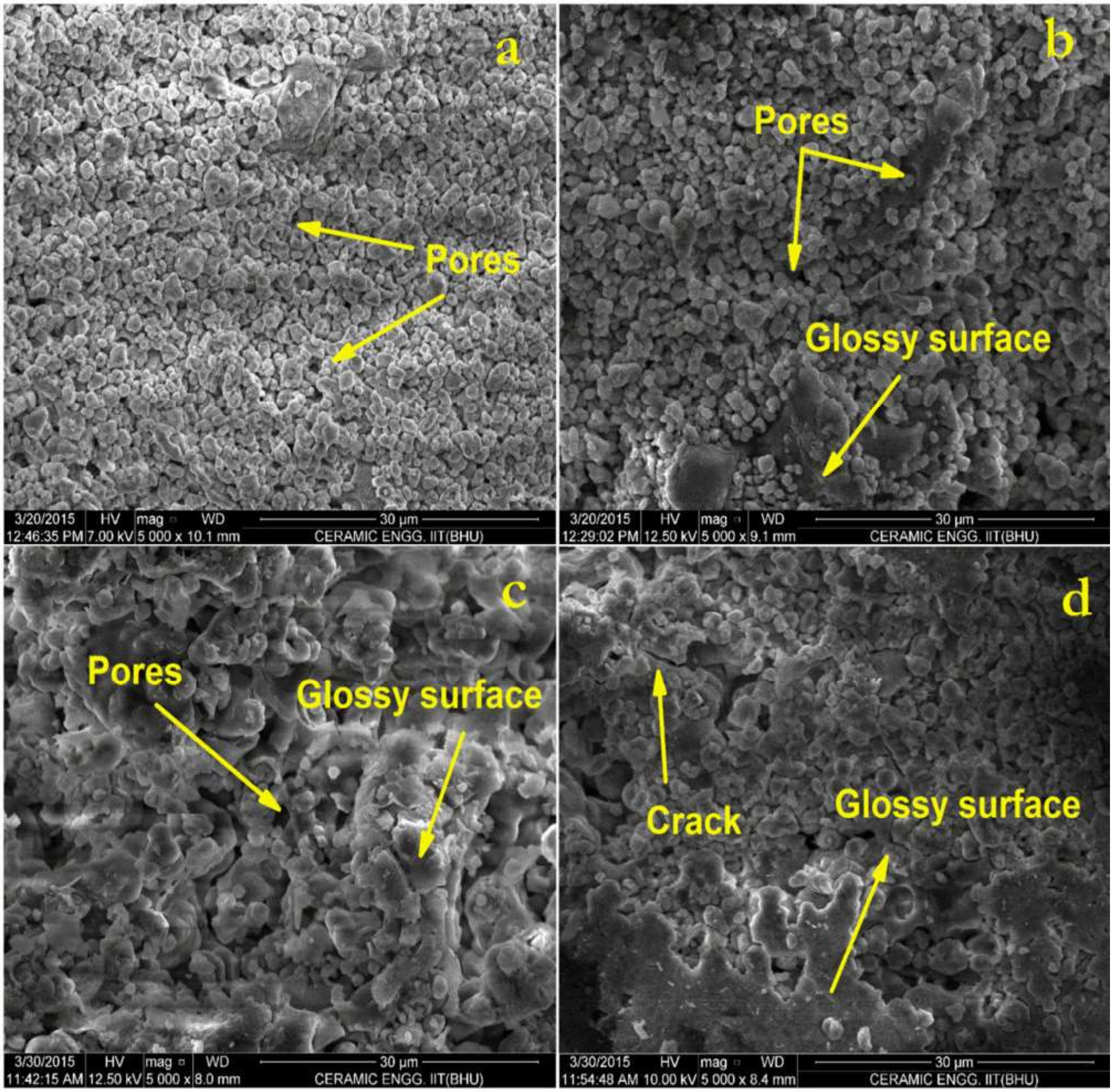
a
Pores
3/20/2015 HV mag WD 30 µm
12:46:35 PM 7.00 kV 5 000 x 10.1 mm CERAMIC ENGG. IIT(BHU)
b
Pores
Glossy surface
3/20/2015 HV mag WD 30 µm
12:29:02 PM 12.50 kV 5 000 x 9.1 mm CERAMIC ENGG. IIT(BHU)
c
Pores
Glossy surface
3/30/2015 HV mag WD 30 µm
11:42:15 AM 12.50 kV 5 000 x 8.0 mm CERAMIC ENGG. IIT(BHU)
d
Crack
Glossy surface
3/30/2015 HV mag WD 30 µm
11:54:48 AM 10.00 kV 5 000 x 8.4 mm CERAMIC ENGG. IIT(BHU)

[redacted]

[redacted]

[redacted]

[redacted]

[redacted]

[redacted]

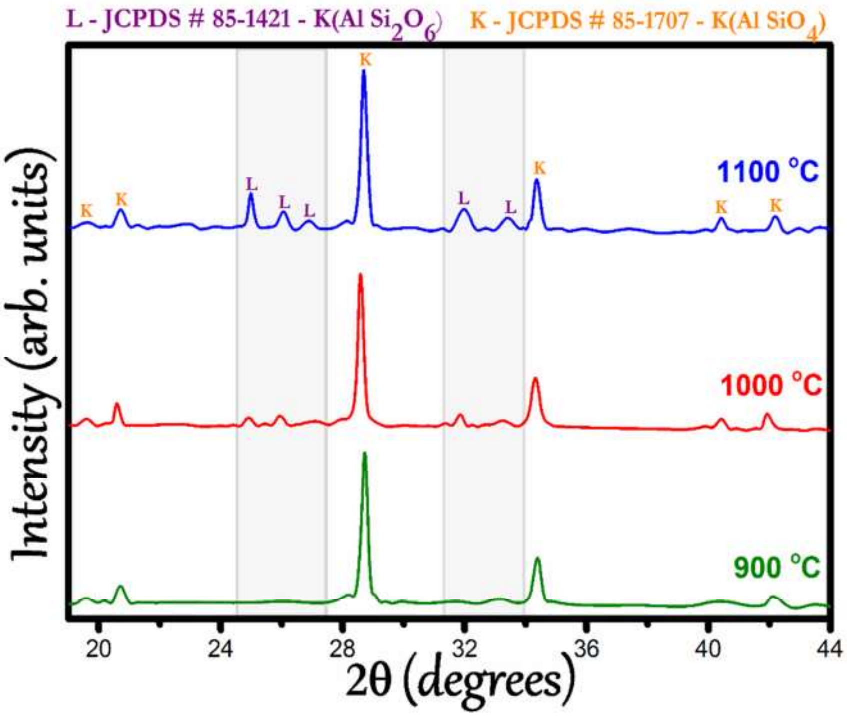

[redacted]

[redacted]

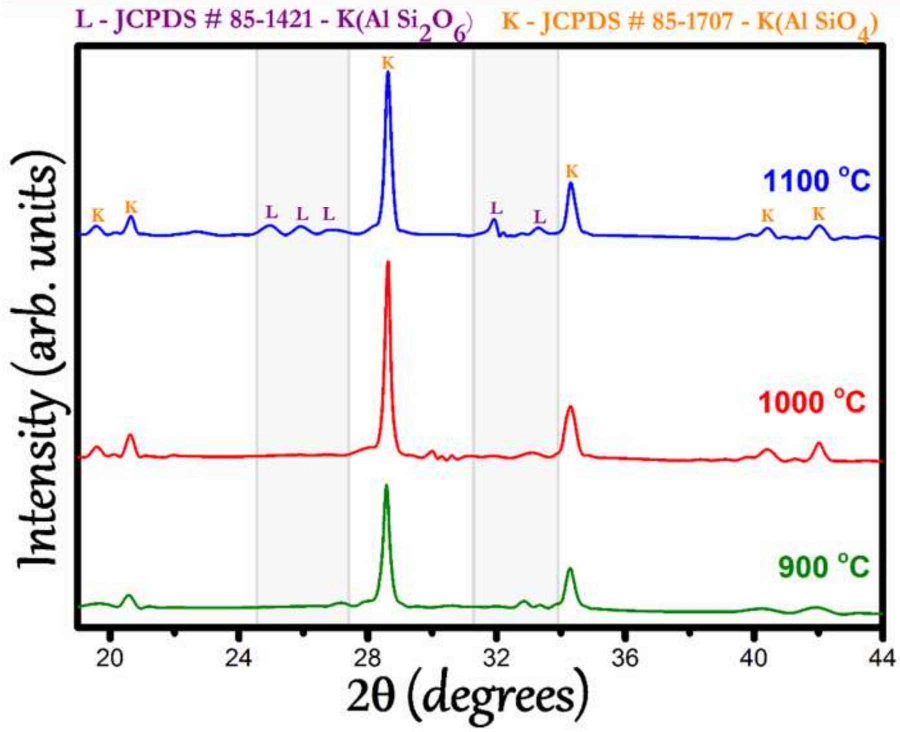
L - JCPDS # 85-1421 - K(Al Si2O6)
K - JCPDS # 85-1707 - K(Al SiO4)
1100 °C
1000 °C
900 °C
Intensity (arb. units)
2θ (degrees)
20
24
28
32
36
40
44

[redacted]

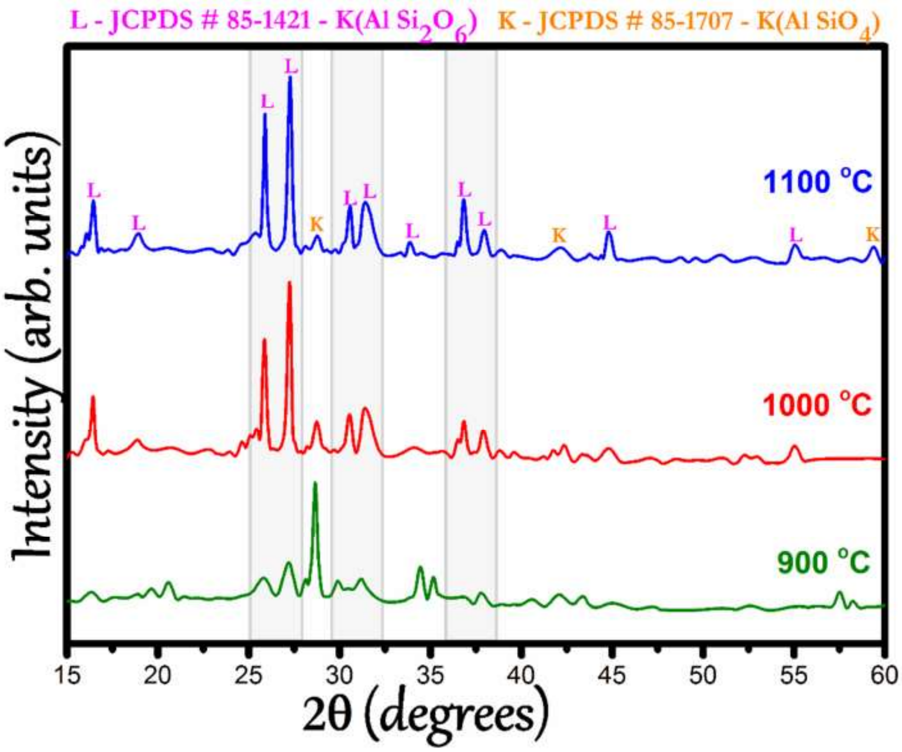

[redacted]

2 [redacted]

[redacted]

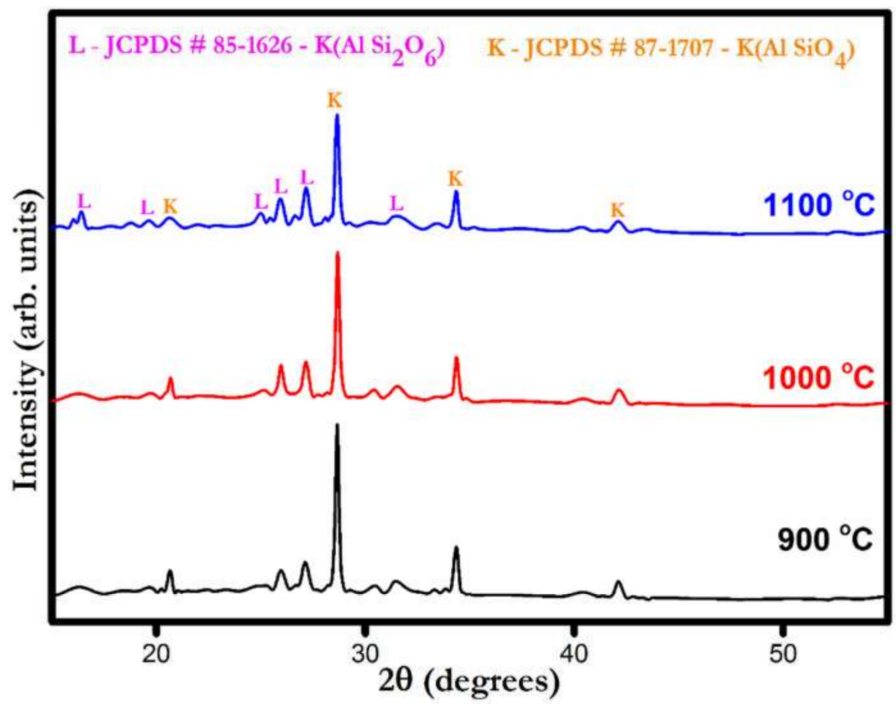

[redacted]

[redacted]

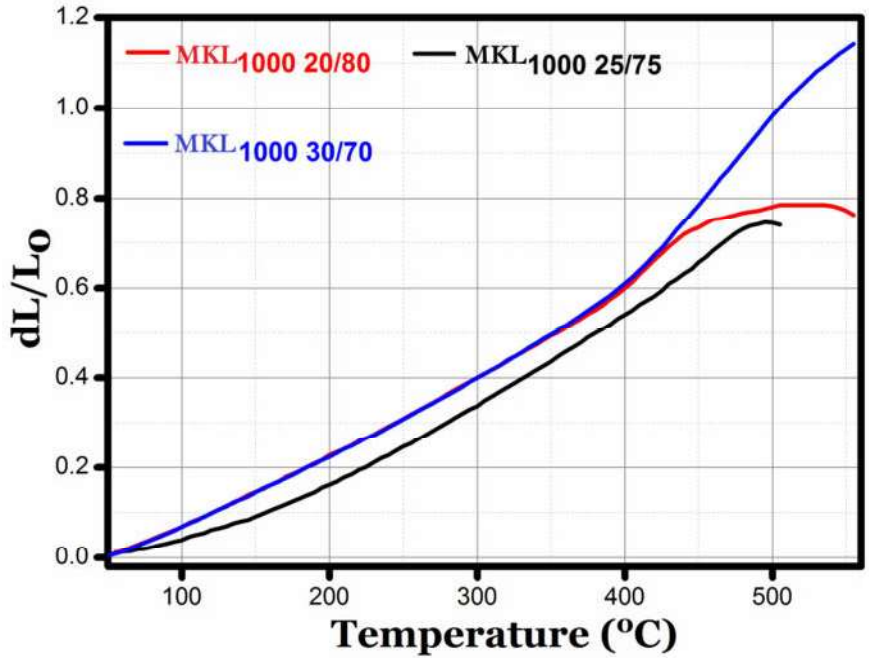

[redacted]

[redacted]

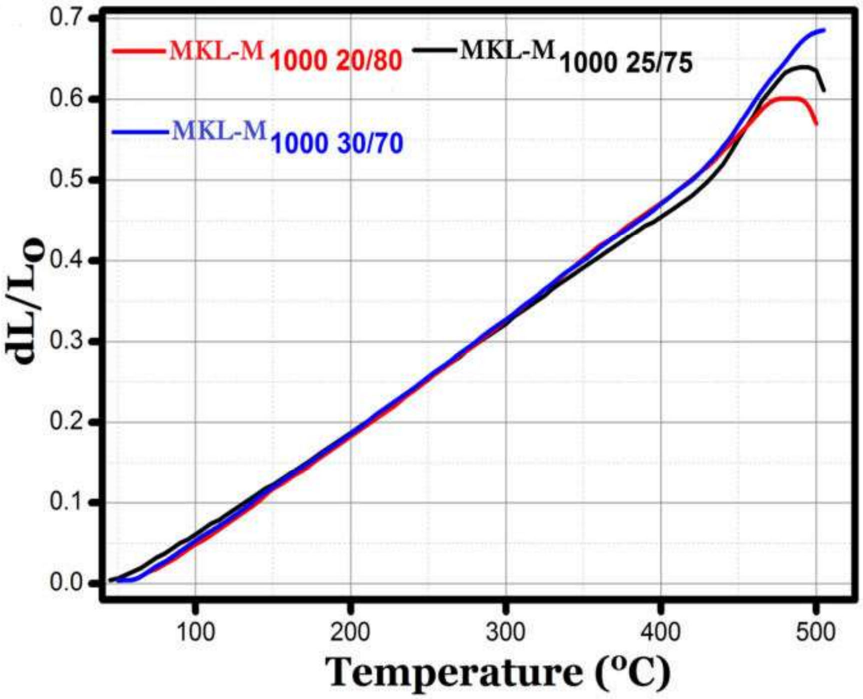
MKL-M 1000 20/80
MKL-M 1000 25/75
MKL-M 1000 30/70
dL/Lo
Temperature (°C)
0.0
0.1
0.2
0.3
0.4
0.5
0.6
0.7
100
200
300
400
500

[redacted]

[redacted]

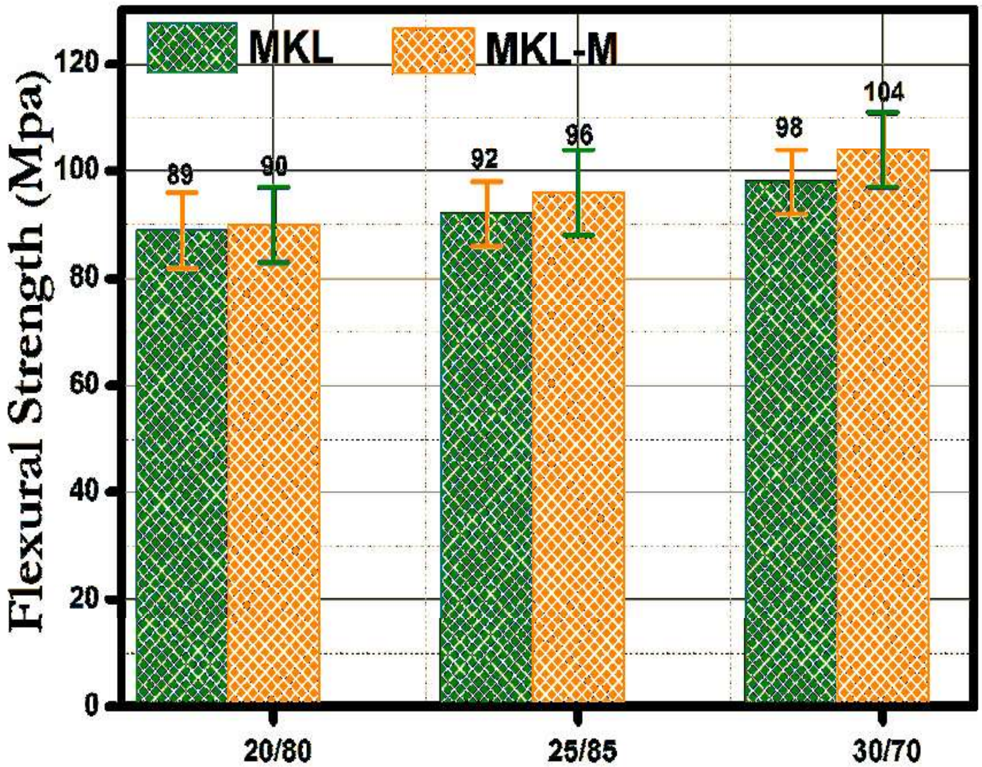

[redacted]

[redacted]

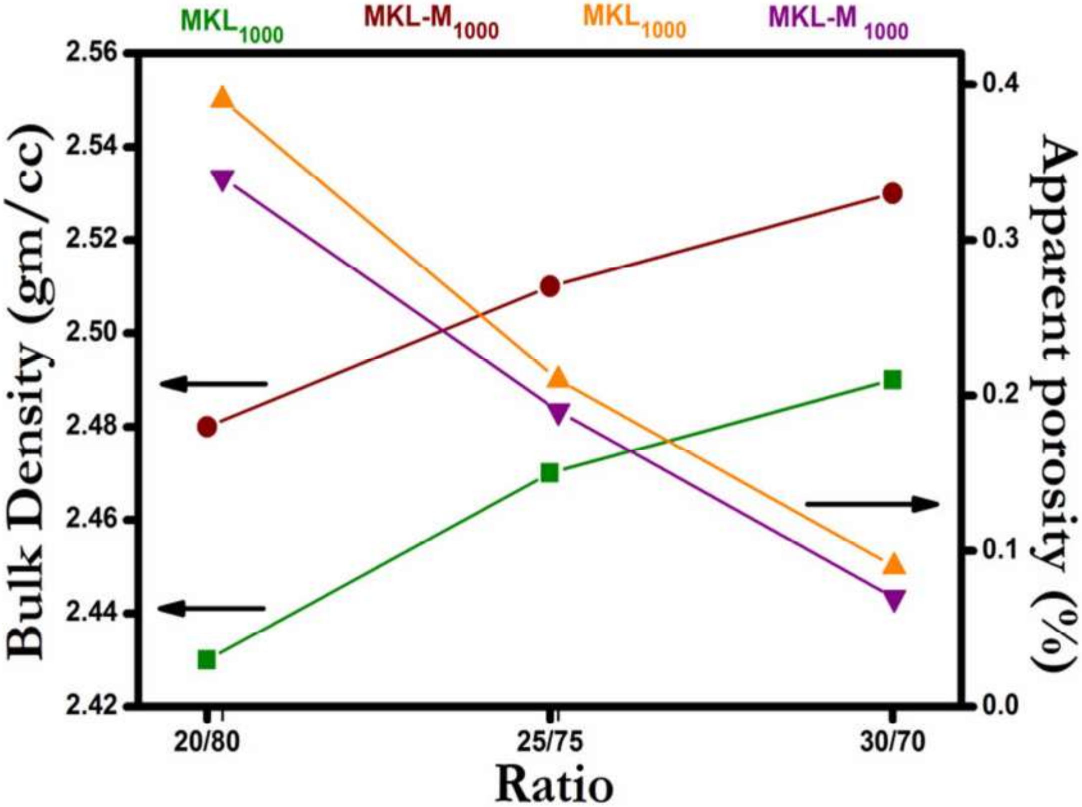
MKL1000
MKL-M1000
MKL1000
MKL-M 1000
Bulk Density (gm/cc)
Apparent porosity (%)
Ratio
20/80
25/75
30/70
2.56
2.54
2.52
2.50
2.48
2.46
2.44
2.42
0.4
0.3
0.2
0.1
0.0

[redacted]

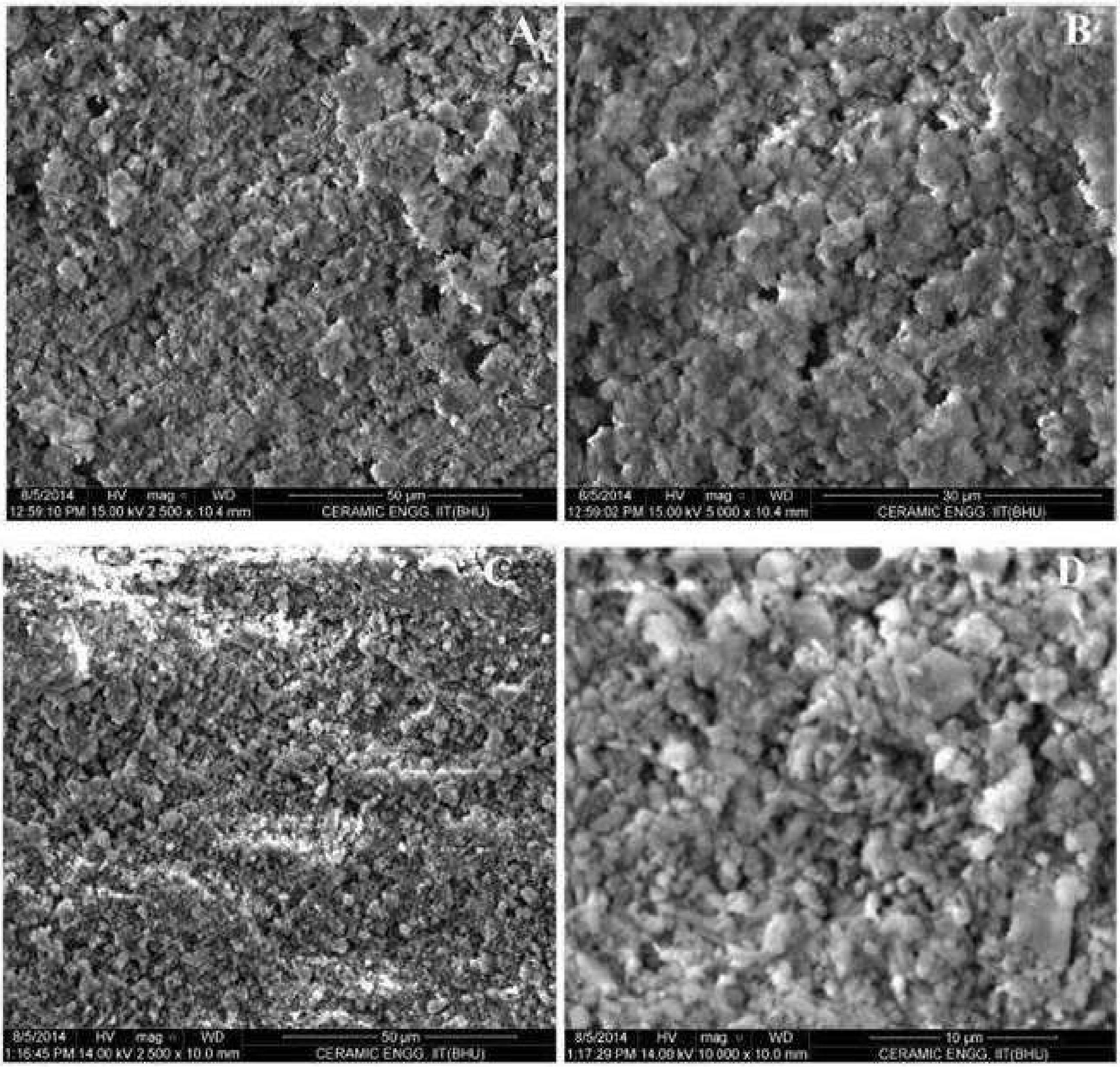
A
B
C
D
8/5/2014 HV mag WD
12:59:10 PM 15.00 kV 2 500 x 10.4 mm
50 µm
CERAMIC ENGG. IIT(BHU)
8/5/2014 HV mag WD
12:59:02 PM 15.00 kV 5 000 x 10.4 mm
30 µm
CERAMIC ENGG. IIT(BHU)
8/5/2014 HV mag WD
1:16:45 PM 14.00 kV 2 500 x 10.0 mm
50 µm
CERAMIC ENGG. IIT(BHU)
8/5/2014 HV mag WD
1:17:29 PM 14.00 kV 10 000 x 10.0 mm
10 µm
CERAMIC ENGG. IIT(BHU)

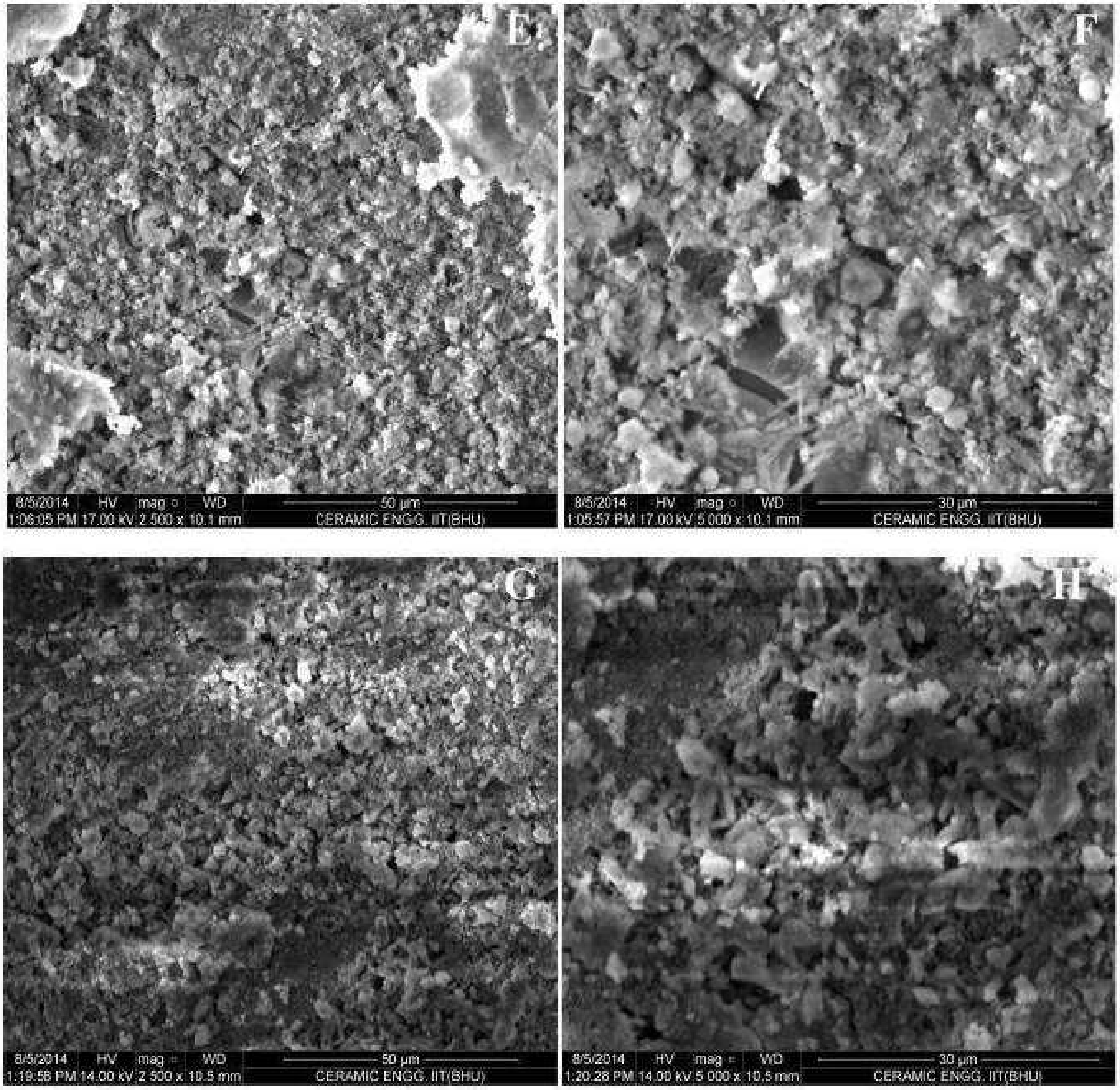
E
F
G
H
8/5/2014 HV mag WD 50 µm
1:06:05 PM 17.00 kV 2 500 x 10.1 mm CERAMIC ENGG. IIT(BHU)
8/5/2014 HV mag WD 30 µm
1:05:57 PM 17.00 kV 5 000 x 10.1 mm CERAMIC ENGG. IIT(BHU)
8/5/2014 HV mag WD 50 µm
1:19:56 PM 14.00 kV 2 500 x 10.5 mm CERAMIC ENGG. IIT(BHU)
8/5/2014 HV mag WD 30 µm
1:20:28 PM 14.00 kV 5 000 x 10.5 mm CERAMIC ENGG. IIT(BHU)

[redacted]

[redacted]

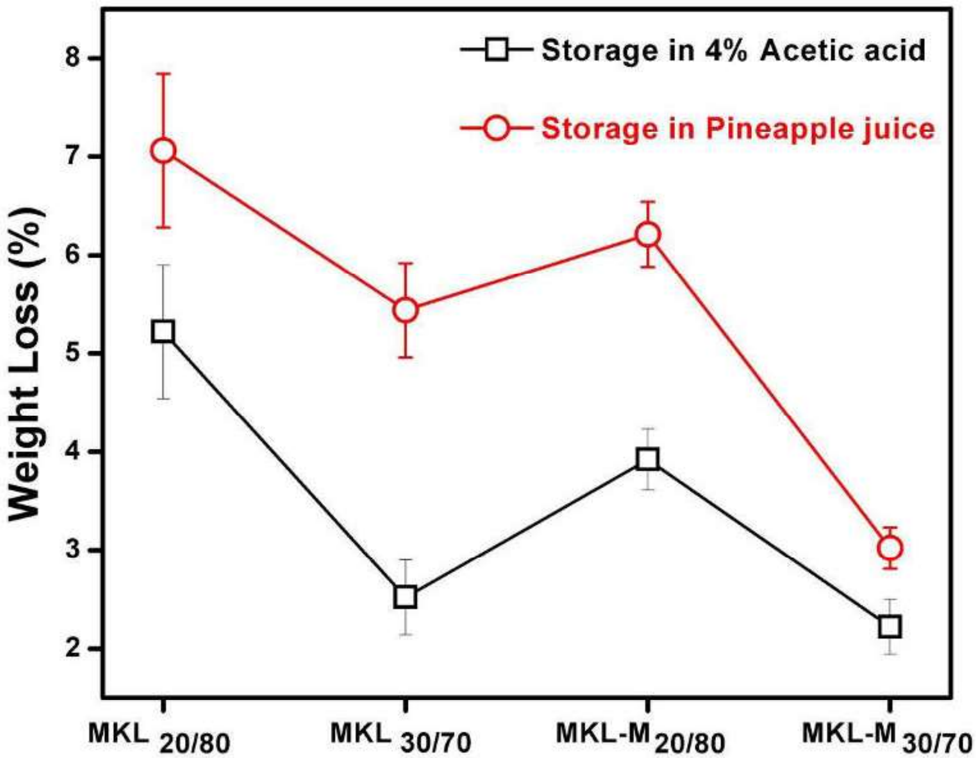

[redacted]

20/80 [redacted]

30/70 [redacted]

$MKL_{20/80}$					
$MKL_{30/70}$					
$MKL\text{-}M_{20/80}$					
$MKL\text{-}M_{30/70}$					

[redacted]

[redacted]

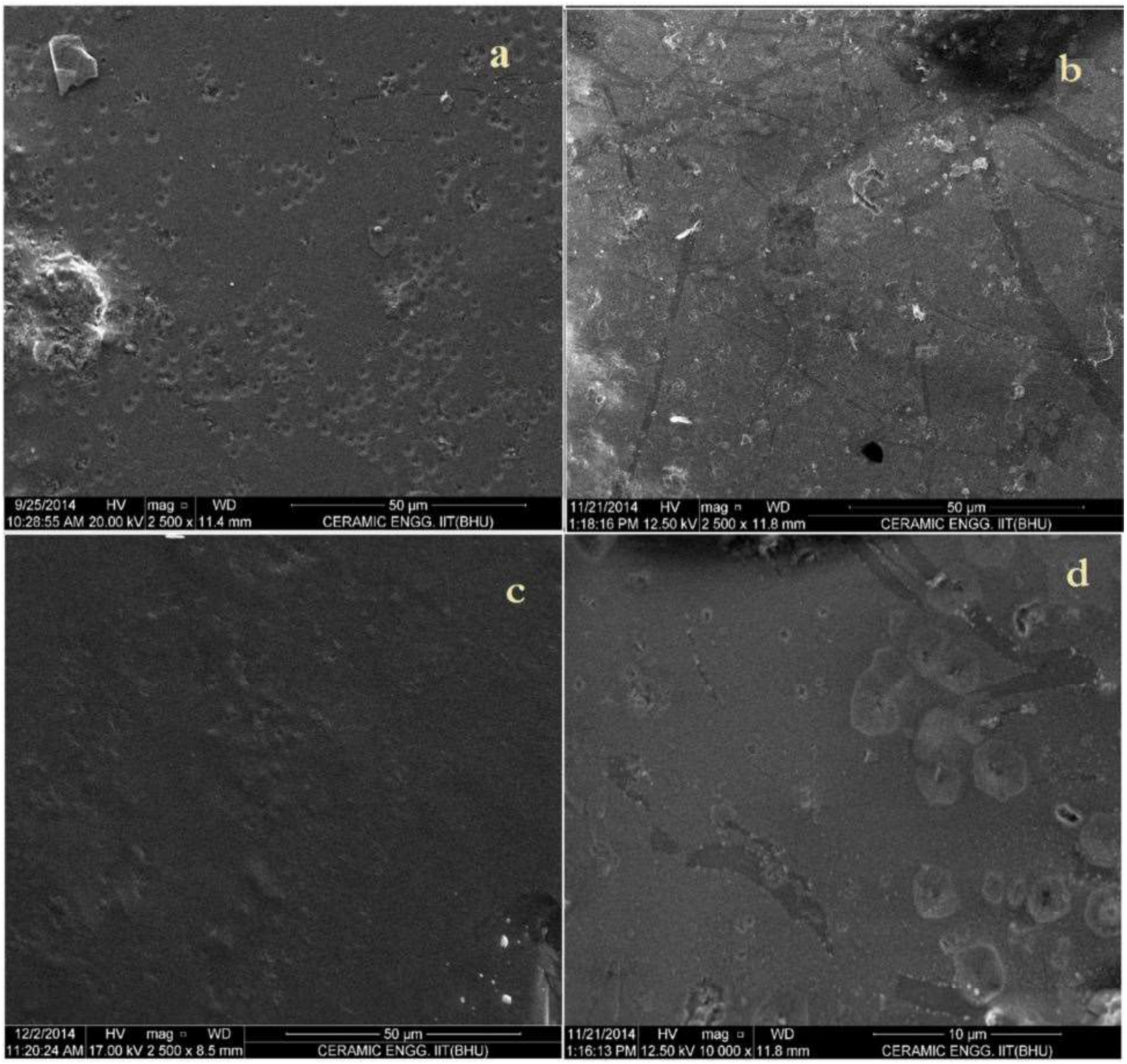

[redacted]

[redacted]

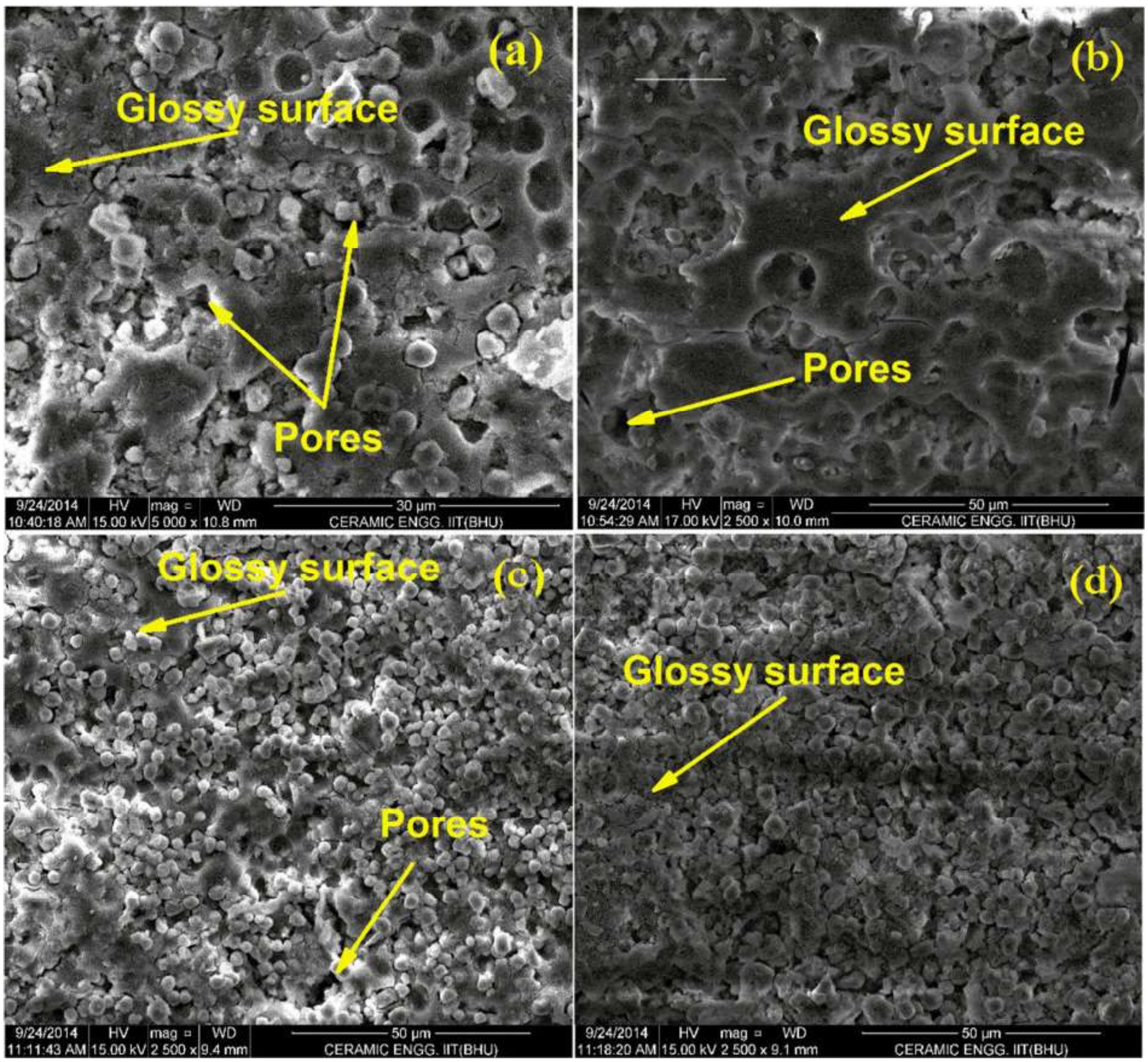

[redacted]

[redacted]

[redacted]

[redacted]

[redacted]

[redacted]

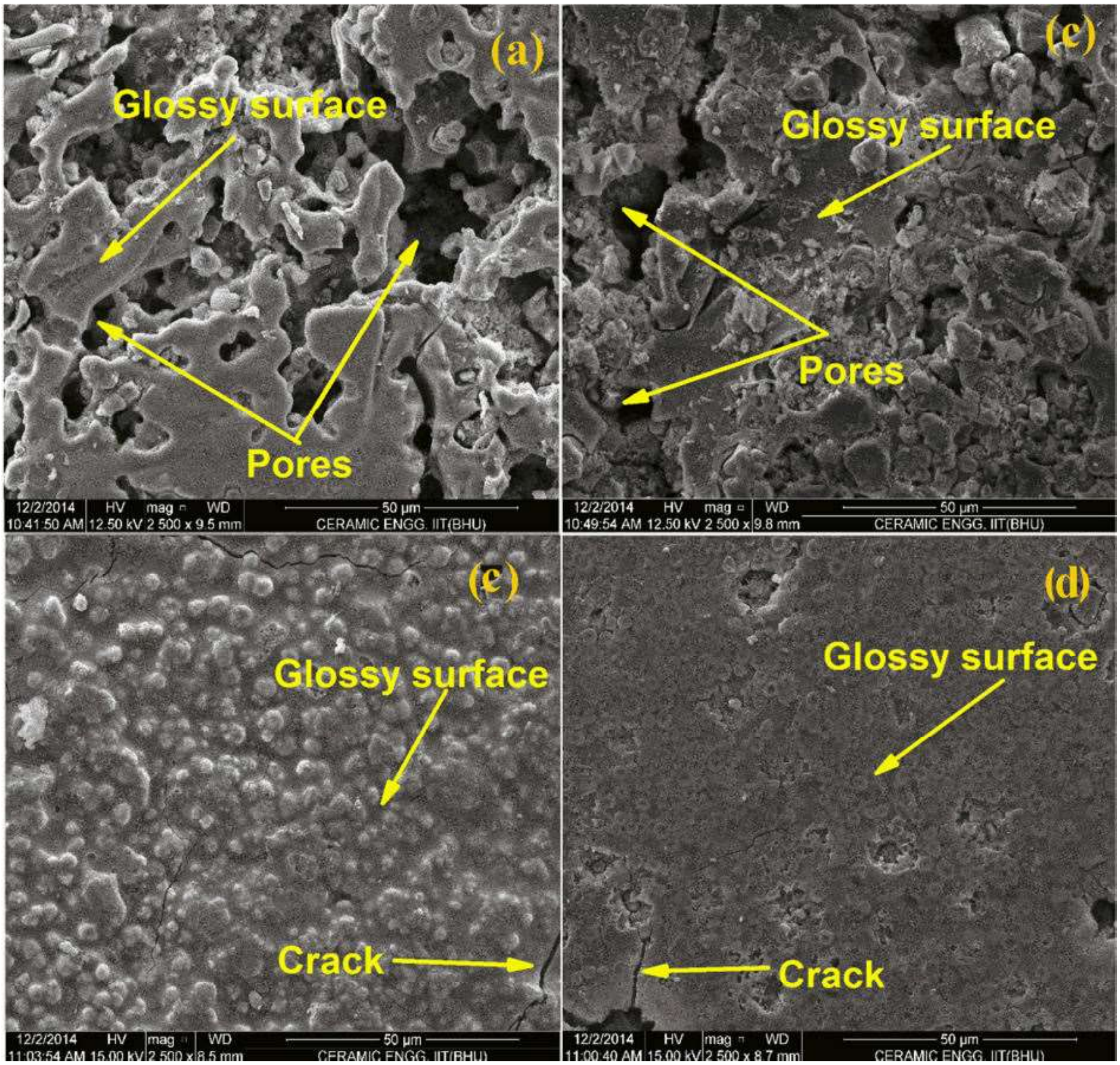

[redacted]

2

2

6 6

+ +

1000 1000

4.3 Mechanochemically Synthesized leucite/kalsilite based bioactive glass ceramic composite for dental veneering

4.3.1 Phase analysis

Phase formation in the leucite and kalsilite composites has been confirmed using XRD. Figs. 4.25 & 4.26 show the XRD patterns of the leucite glass ceramic composites with & without CaF_2 before and after heat treatment. Before heat treatment, diffraction peaks are well matched to the JCPDS card No. 71-1147 of leucite with the unit cell parameters a = b =13.09 and c = 13.75 Å (Figs. 4.25 & 4.26).

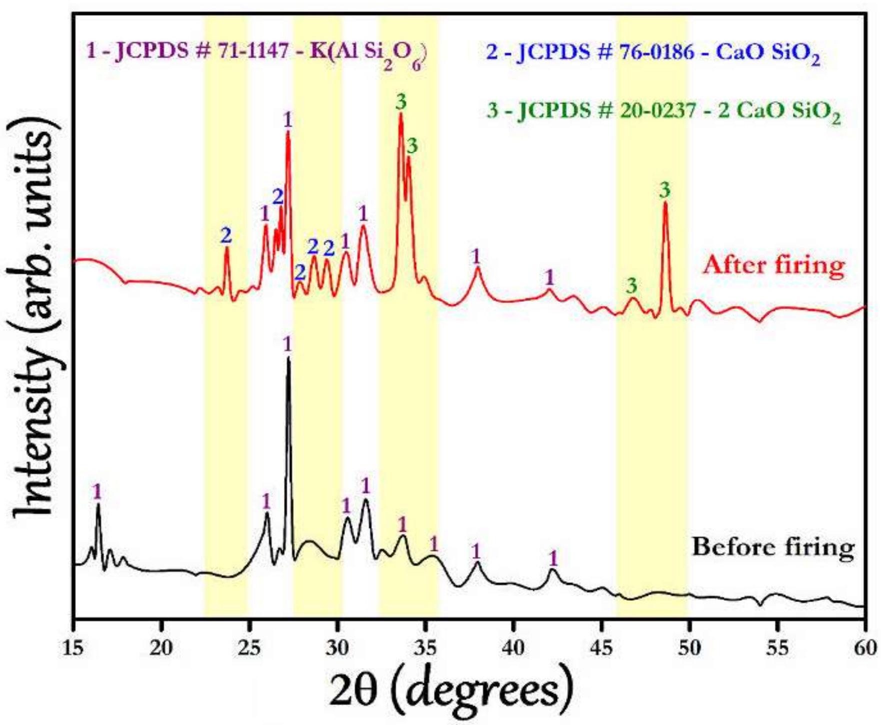

Fig. 4.25 XRD pattern of COMP-1 before and after heat treatment up to 960 °C

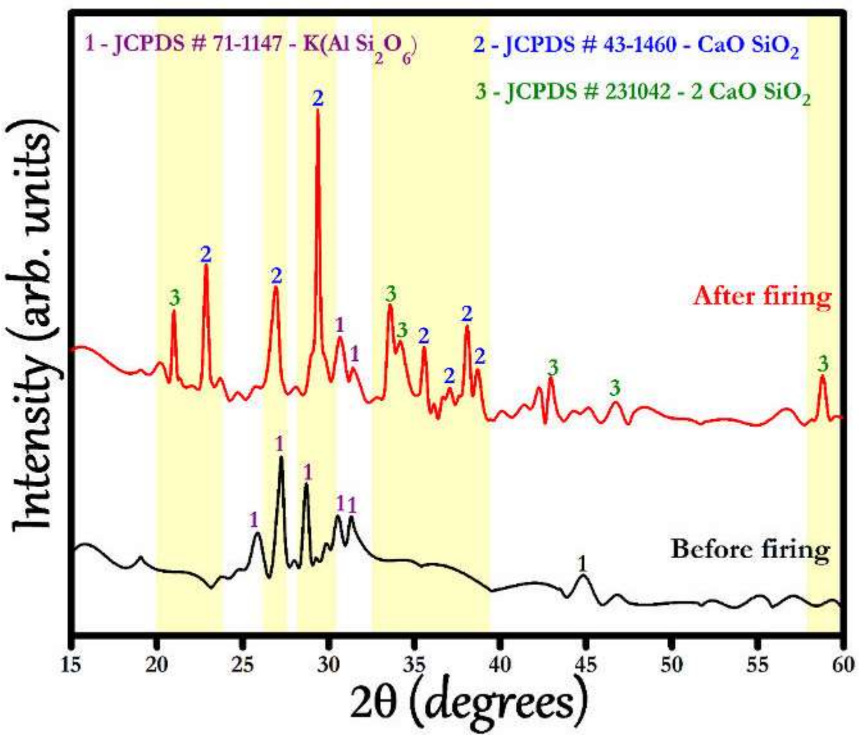

Fig. 4.26 XRD pattern of COMP-2 before and after heat treatment up to 960 °C

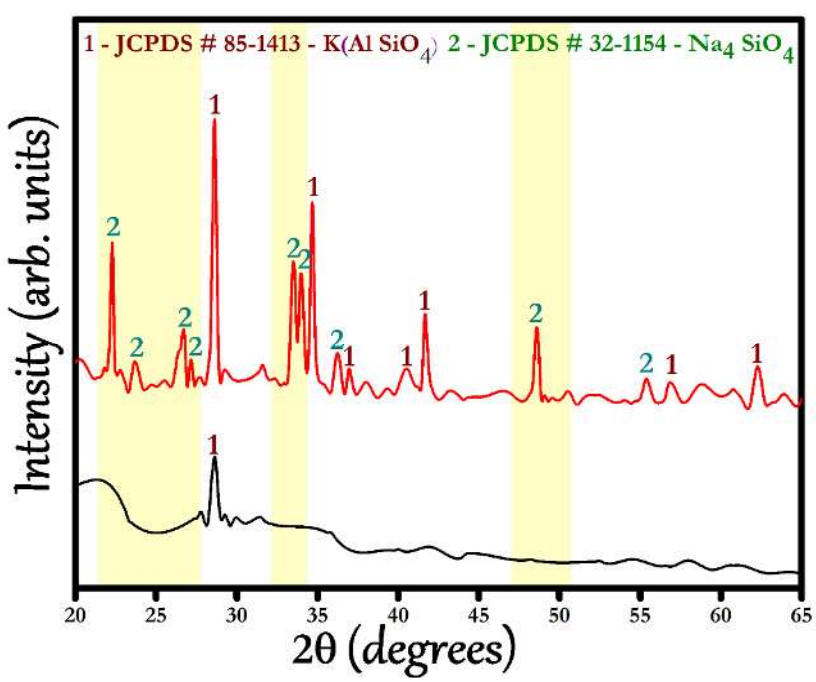

Fig. 4.27 XRD pattern of COMP-3 before and after heat treatment up to 960 °C

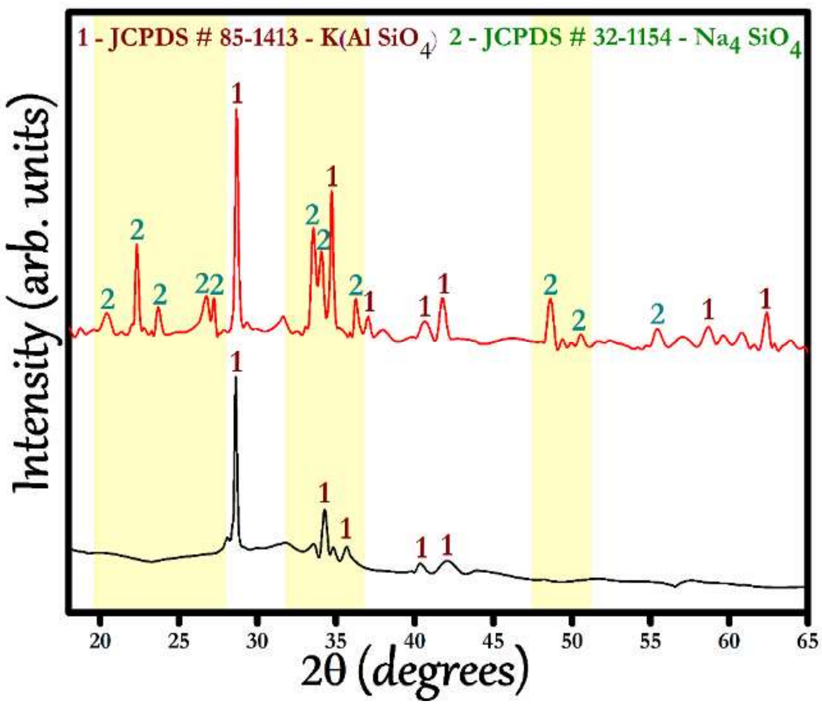

Fig. 4.28 XRD pattern of COMP-4 before and after heat treatment up to 960 °C

It is noted from Fig. 4.25 & 4.26 that after heat treatment, a calcium silicate ($2CaO.SiO_2$) and wollastonite ($CaO.SiO_2$) crystalline phases has been observed in both the leucite composites (COMP-1 & COMP-2). The Intensity of the peaks corresponding to leucite phase has been reduced after heat treatment accompanying with the formation of another two phases, calcium silicate and wollastonite. It is also seen from Fig. 4.26 that formation of wollastonite phase is higher in the case of COMP-2 (after heat treatment) than that of COMP-1. Formation of the $2CaO.SiO_2$ and $CaO.SiO_2$ crystalline phases may lead to improving the flexural strength. This is because these phases have high flexural strength.

Figs. 4.27 & 4.28 show the XRD patterns of the kalsilite glass ceramic composites with & without MgF_2 (before and after heat treatment). Before firing, the diffraction peaks are well matched to the JCPDS card No. 85-1413 of kalsilite phase. Some amorphous phase is also seen in the XRD patterns. After firing, a sodium orthosilicate ($2Na_2O.SiO_2$) crystalline phase has been found in both the composites (COMP-3 & COMP-4) along with the kalsilite phase.

4.3.2 Coefficient of thermal expansion (CTE)

Thermal compatibility is the most essentials for veneering glass-ceramic fused to metal restorations. Fig. 4.29 shows the thermal expansion behavior of all the leucite and kalsilite bioactive glass ceramic composites along with the commercial Dentine A2.

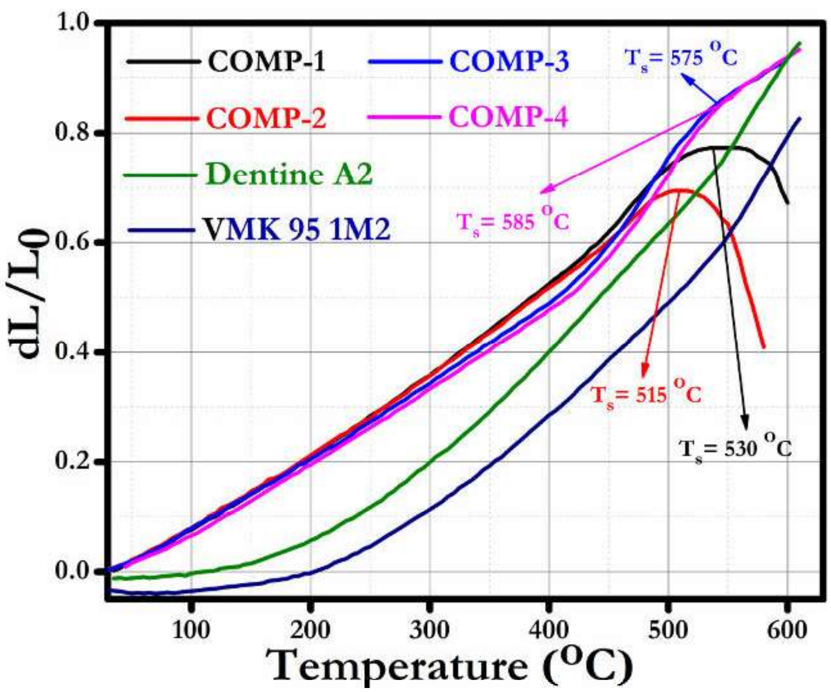

Fig. 4.29 CTE curves of COMP-1, COMP-2, COMP-3 and COMP-4 along with commercial Dentine A2 and substrate

The values of CTE have been found to be 15.6×10^{-6}, 14.5×10^{-6}, 15.9×10^{-6} and 15.6×10^{-6} /°C for the samples COMP-1, COMP-2, COMP-3 and COMP-4 respectively.

These values are similar to the values obtained for dentine (VITA VMK 95 Dentin 1M2) and the opaque layer (VITA VMK95 opaque 1M2) as 14.5×10^{-6} /°C & 14.0×10^{-6}/°C respectively. The values of CTE for both the substrate and the composite are very close therefore applied heat treatment will not lead to peel off the coating. The composition COMP-2 has slightly low CTE than that of COMP-1. It is because of that more Ca^{2+} ions enter into leucite lattice at high temperature and lower the CTE [Zhang Y. *et al.* 2006]. Leucite and kalsilite have a high CTE value, therefore, increase the overall thermal expansion of the dental ceramic compatible with the metals [Hashimoto S. *et al.* 2005].

4.3.3 Flexural strength

Fig. 4.30 shows the flexural strength of all the composites and commercial dentine A2. The prepared composite samples show the flexural strength comparable to that of the commercial dentine. This is due to the formation of the crystalline calcium silicate and wollastonite phases (after heat treatment) in the leucite based composites and sodium orthosilicate in the kalsilite based composites. It is noted from Fig. 4.30 that the composition COMP-2 has the high flexural strength than that of COMP-1. This is in conformity with the CTE results that COMP-2 has low CTE than that of COMP-1. It leads to increase in the flexural strength.

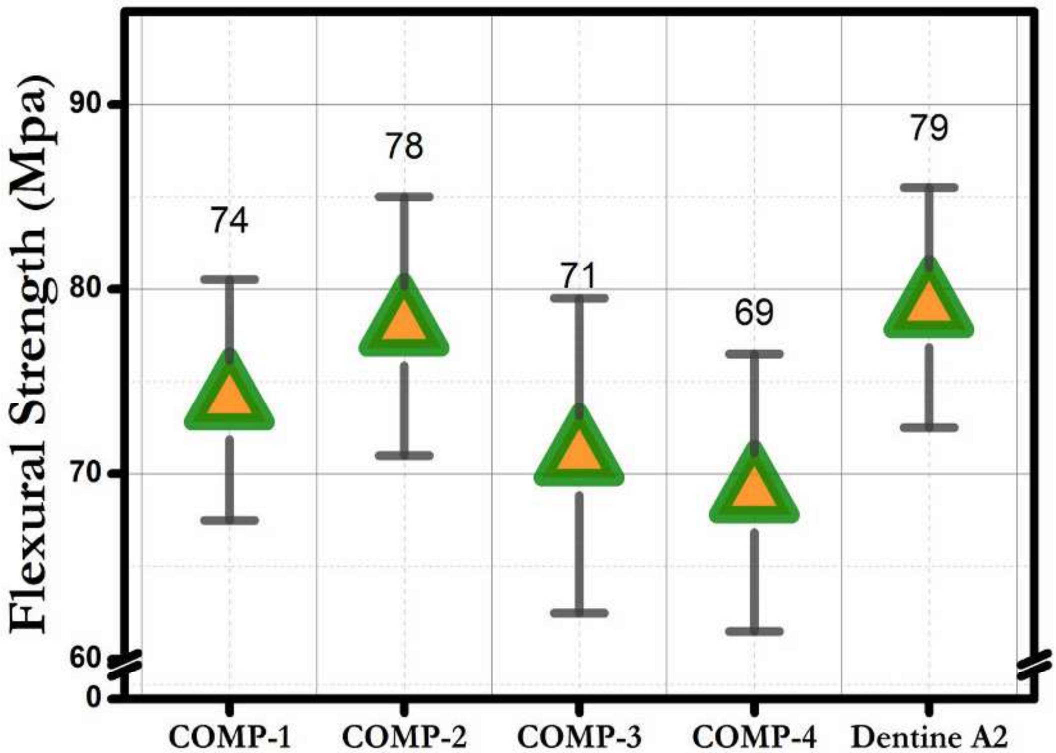

Fig. 4.30 Flexural strength of COMP-1, COMP-2, COMP-3, COMP-4 and commercial dentine

Composition COMP-3 and COMP-4 has the low flexural strength than that of COMP-2. This is because sodium orthosilicate ($2Na_2O.SiO_2$) has less strength as compared to the calcium silicate and wollastonite [Al-Noaman A. *et al.* 2013].

It is also noted that composition, COMP-4 has less flexural strength than that of the COMP-3. This is because the concentration of sodium orthosilicate phase is slightly higher in COMP-4 than that in the COMP-3 (Figs. 4.27 & 4.28). This leads to decrease in the flexural strength of COMP-4.

4.3.4 Interface layer of the composites and the substrate

Fig. 4.31 shows the surface morphology of the interface layer between the composite and the substrate (composite coated substrate). It confirms a perfect attachment between the substrate and the composite coating. There is no micro crack and peeling throughout the interfaces. Compression interface bond depends on the geometry of CTE of the substrate. The firm attachment of the bioactive coating on the substrate has been ascribed to the well matched CTE.

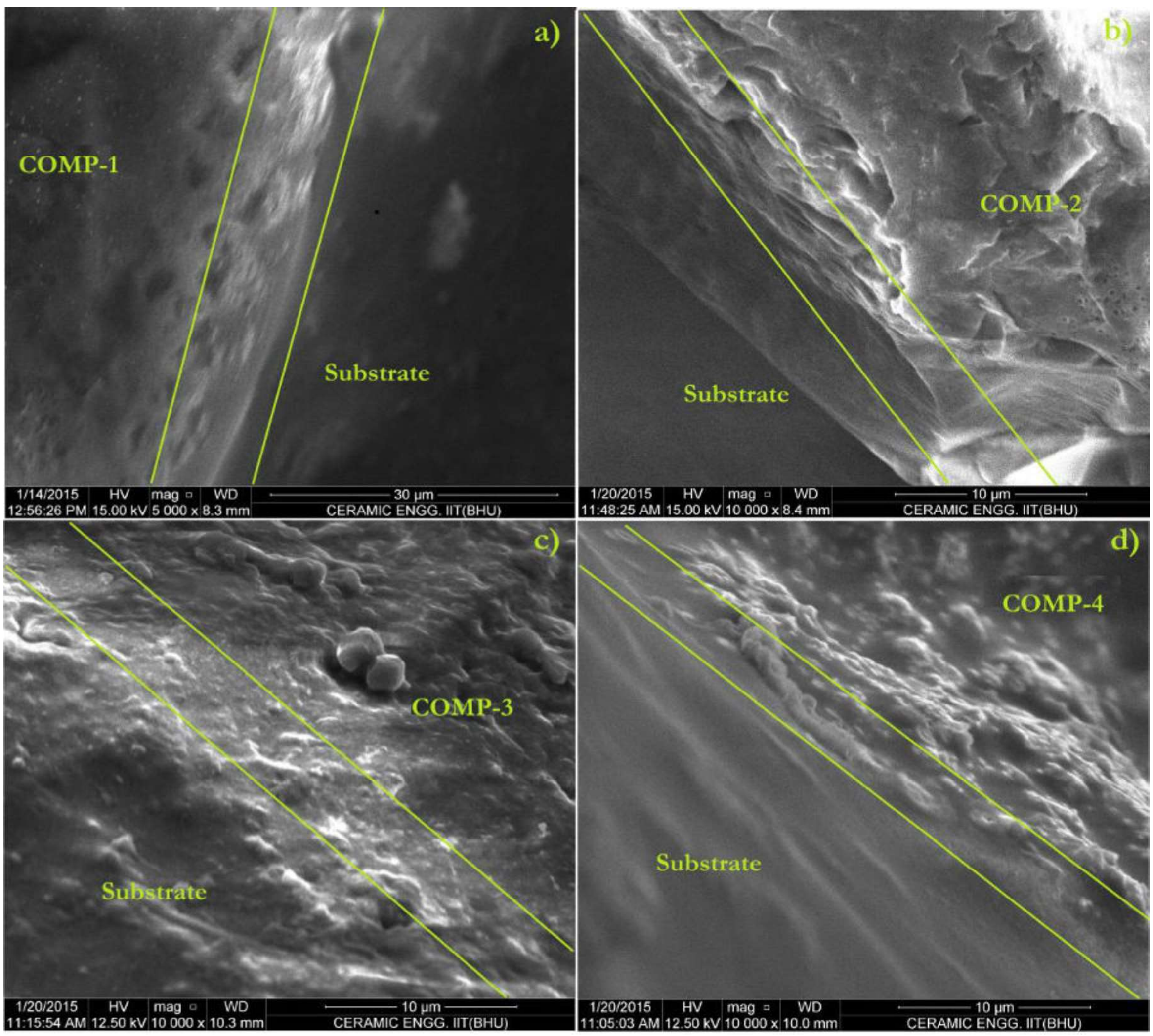

Fig. 4.31 SEM image showing the surface morphology of interface layer between the composites and the substrate

4.3.5 Bioactivity in SBF

The capability of hydroxyapatite layer formation has been investigated on the bioactive glass ceramic composites through immersion in SBF for 0, 7 and 14 days soaking time.

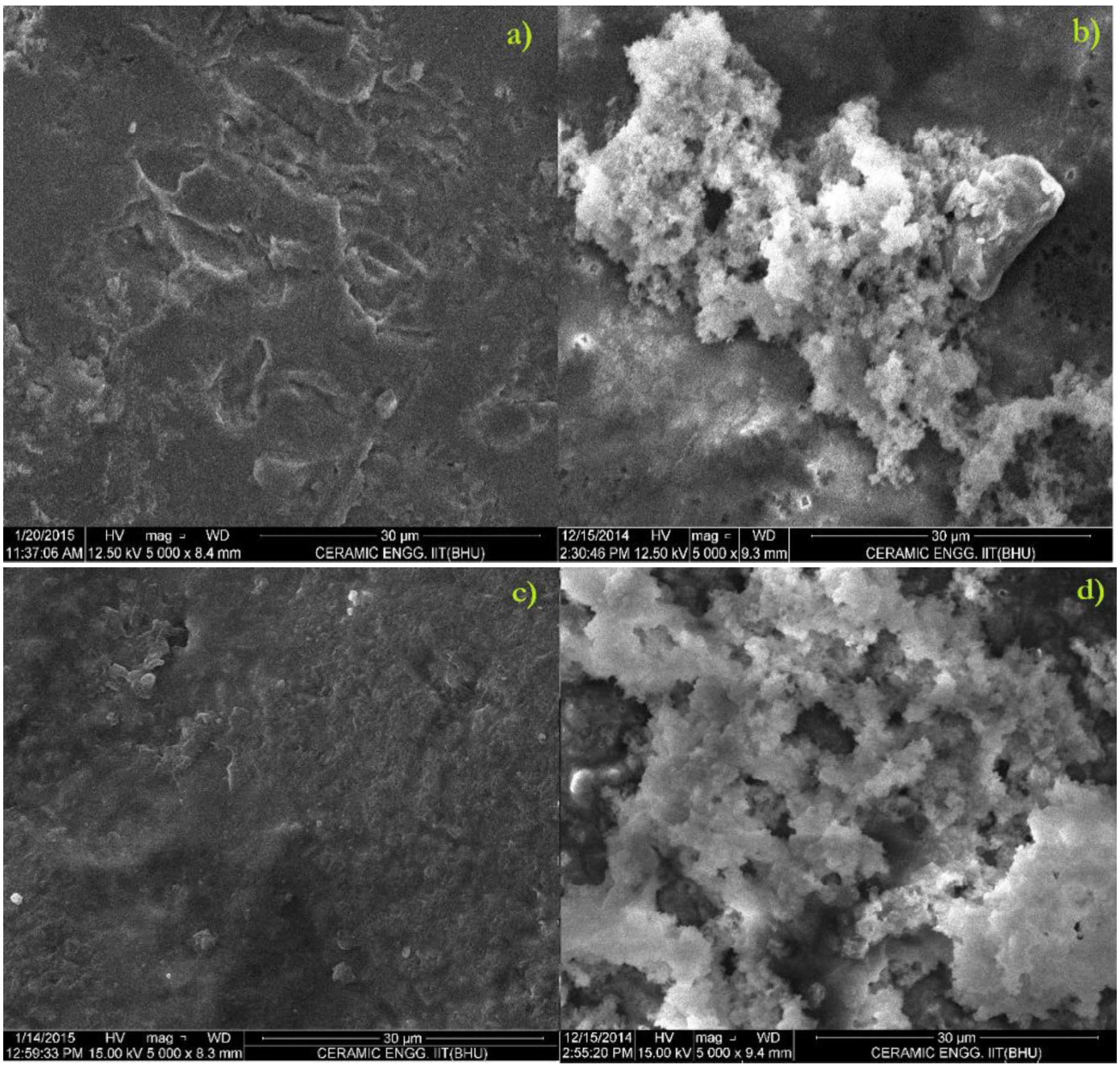

Fig. 4.32 SEM images of the coated specimens of COMP-1 (a) before (b) after immersion for 7 days in SBF, COMP-2 (c) before and (d) after immersion for 7days in SBF showing HAp formation

The surface of the specimens before and after immersion in SBF has been examined by SEM (Fig. 4.32). The hydroxyapatite layer covers the whole surface of all the composite samples, has been observed after 7 days soaking in SBF (Fig. 4.32a to 4.32h). FTIR has analyzed all composite samples soaked in SBF.

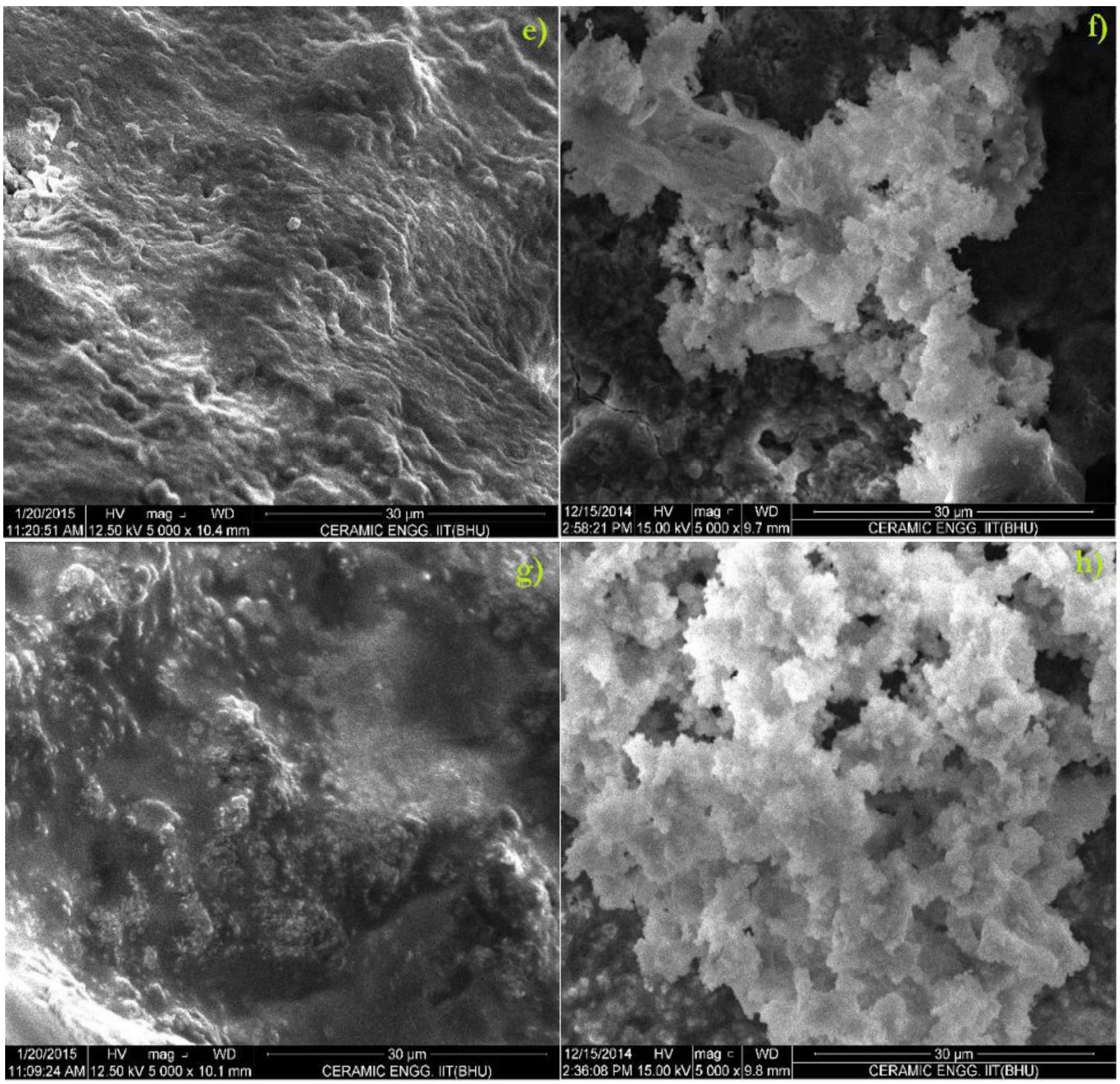

Fig. 4.32 SEM images of the coated specimens of COMP-3 (e) before and (f) after immersion for 7 days in SBF showing HAp formation, COMP-4 (g) before and (h) after immersion for 7 days in SBF showing HAp formation

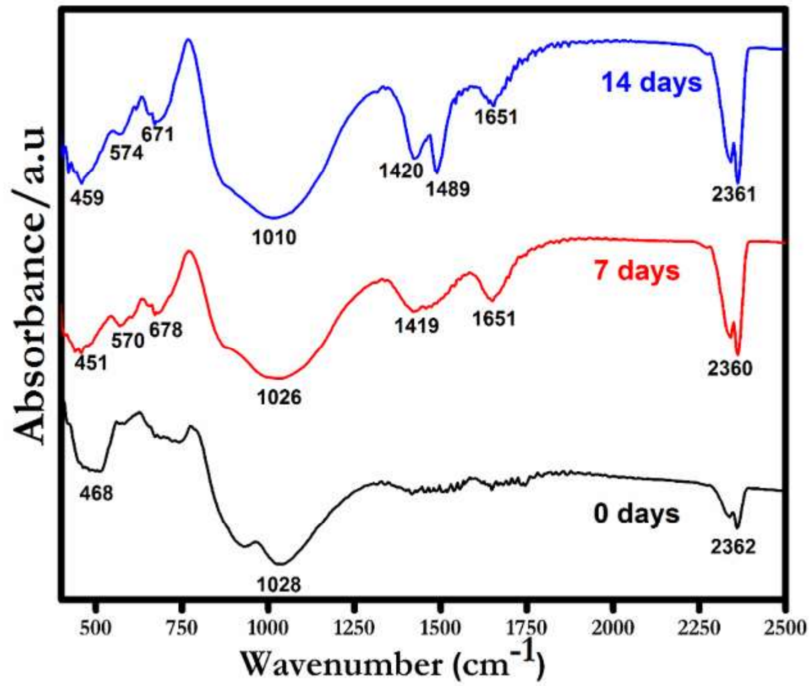

Fig. 4.33 FTIR absorbance bands of COMP-1 composite before and after immersion in SBF for 0, 7 and 14 days

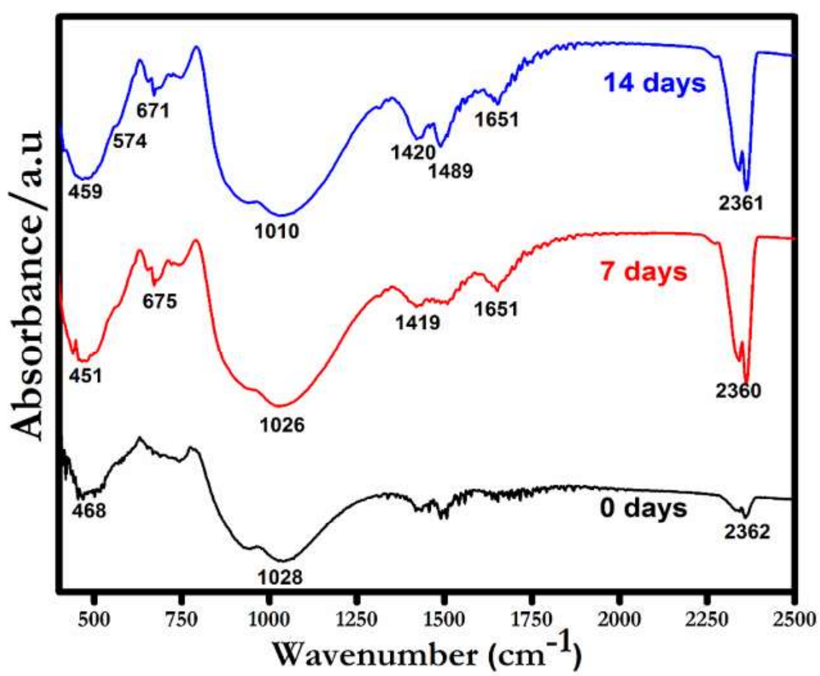

Fig. 4.34 FTIR absorbance bands of COMP-2 composite before and after immersion in SBF for 0, 7 and 14 days

Figs. 4.33 to 4.36 show the FTIR transmittance bands of the composites before and after immersion in SBF for 0, 7 and 14 days. Intense peaks in the wavelength range 1150–900 and 650–500 cm^{-1} is observed due to stretching vibrations of the phosphate (PO_4^{-3}) groups (after soaking in SBF for 7 days at 37 °C). The low intense peaks appeared in the range 1500–1400 cm^{-1} indicates the presence of CO_3^{-2} molecules in the sample.

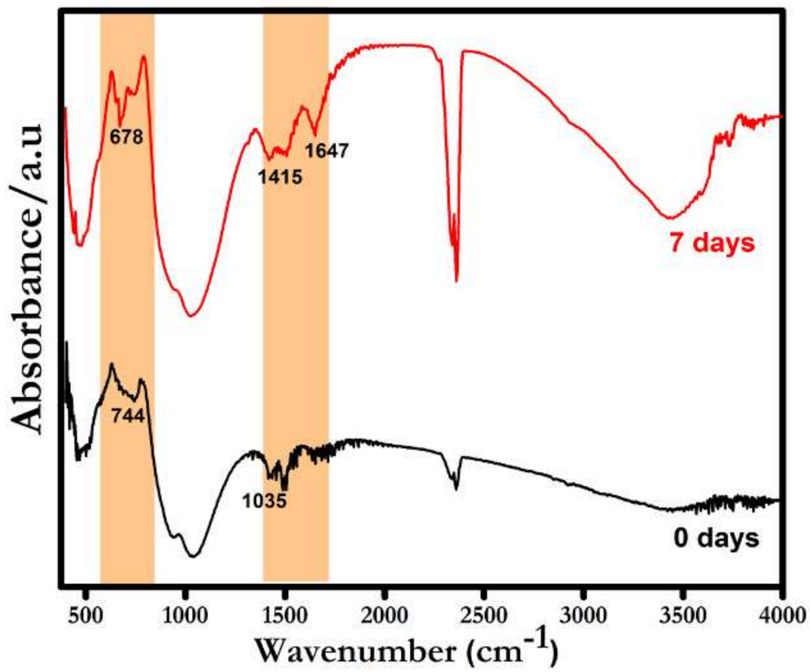

Fig. 4.35 FTIR absorbance bands of COMP-3 composite before and after immersion in SBF for 0 and 7 days

There is also an additional peak at 450 cm^{-1} assigned to the bending vibration mode of Si-O bond. The results of SEM are also in conformity with the results of FTIR. Since in the 1990s, wollastonite ($CaSiO_3$) ceramics have been studied as biomaterials for artificial bones and dental roots because wollastonite exhibits excellent bioactivity and biocompatibility. Some investigators have been reported that wollastonite and pseudo-wollastonite ceramics are bioactive and observed that the formation of apatite on the

$CaSiO_3$ ceramics is faster than that on the other bioglass and glass-ceramics in SBF [Noaman A.A. *et al.* 2013].

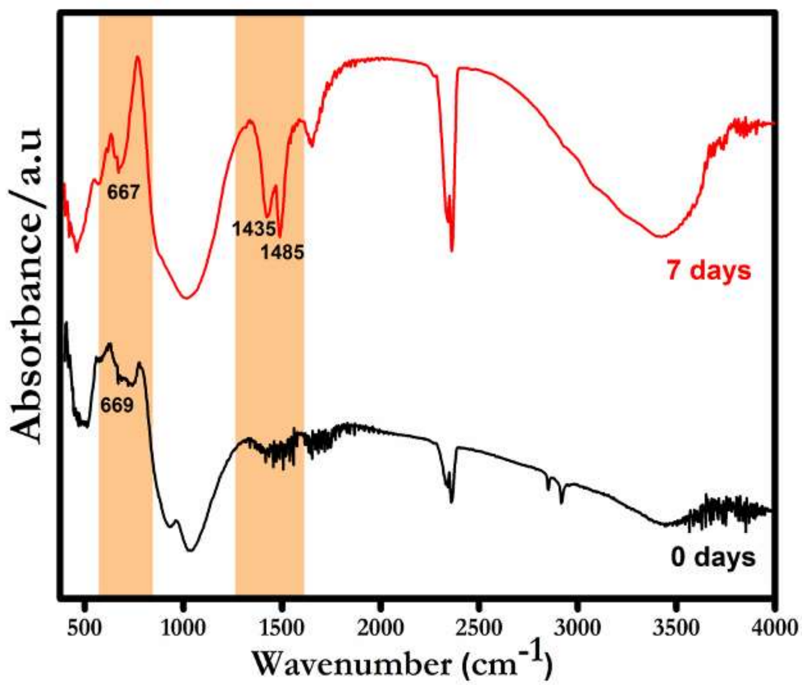

Fig. 4.36 FTIR absorbance bands of COMP-4 composite before and after immersion in SBF for 0 and7 days

Siriphannon et al. have reported that the rate of hydroxyapatite (HA) formation on the pure $CaSiO_3$ ceramic surface is faster than that on the biocompatible apatite-wollastonite A/W glass-ceramics and some other bioactive glass-ceramics [Siriphannon P. *et al.* 1999].

4.3.6 Effect of composite materials on viability and cellular growth inhibition

Higher concentrations of leucite and kalsilite glass-ceramic composites causes partial loss of cell viability in SCC-25 cells although lower concentrations of all the compounds are relatively tolerant to the cells (Fig. 4.37 A). At 10 mg/ml, the cell viability is recorded around 80% and reduces with increasing the concentration (Fig. 4.37 A). A moderate level of growth inhibition has also been observed in SCC-25 cells with the compound of higher concentrations while low concentrated compounds are found to be safe and have no effect on cellular proliferation (Fig. 4.37 B). This suggests a broad spectrum usefulness of the compounds (Fig. 4.37 B). Growth inhibition with kalsilite glass ceramic materials at a fixed concentration (10 mg/ml) for longer periods (72h) causes a moderate retardation (20%) of cell growth compared to treatment for 18h (Fig. 4.37 C).

Interestingly prepared composite materials to perform better as compared to the standard material on inhibition of cell proliferation (Fig. 4.37 C). The direct cellular cytotoxicity test has also been performed with leucite and kalsilite glass–ceramic composites against SCC-25 cells (Fig. 4.37 D). As compared to the higher concentration (50 mg/ml), the low concentrations of leucite and kalsilite glass–ceramic composites are tolerant to the SCC-25 cells and causes significantly less celllysis (Fig. 4.37 D). The results show that leucite and kalsilite glass–ceramic composites are cytocompatible and relatively nontoxic to buccal epithelial cells.

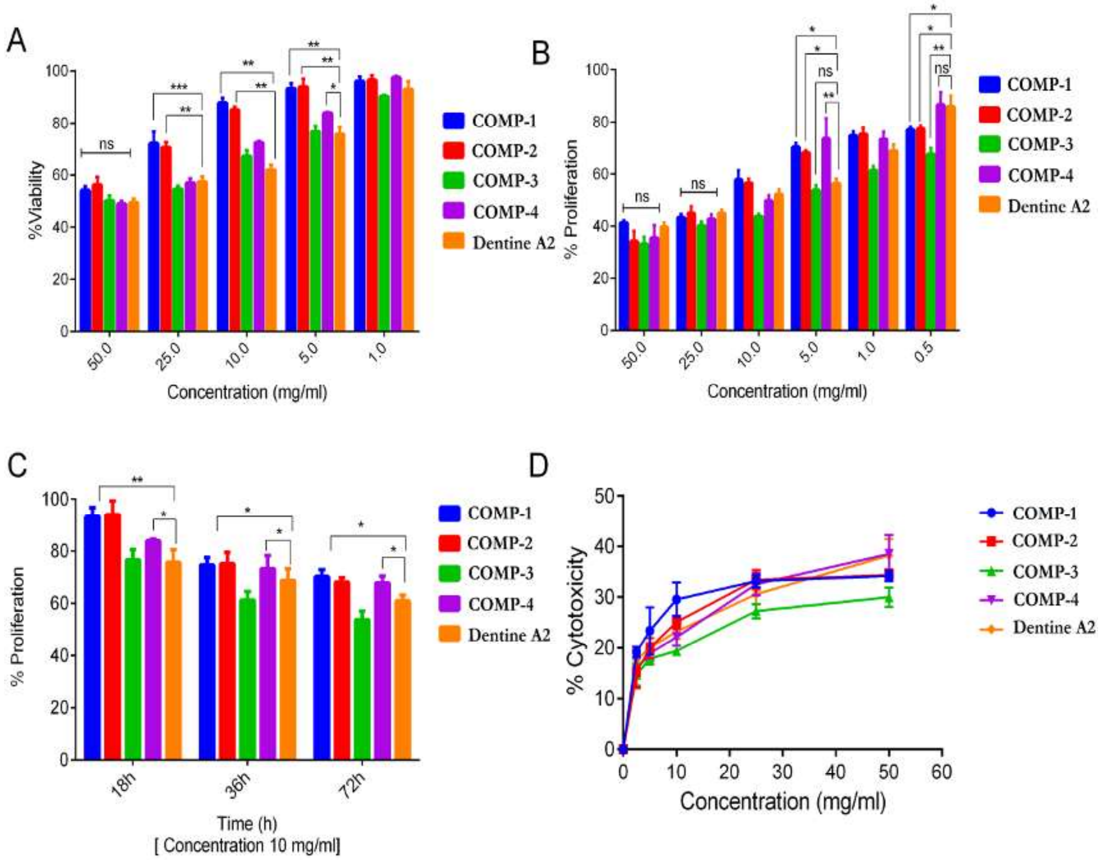

Fig. 4.37 Higher concentration of composite materials retards the growth of SCC-25 cells. (A) The viability of SCC-25 cells in the presence of COMP-1, COMP-2, COMP-3 and COMP-4 glass–ceramic composites (B&C) Graphs show concentration response of leucite and kalsilite glass–ceramic composite materials on tumor cell proliferation and growth (D) Direct cellular cytotoxicity by composite materials against SCC-25 cells. Data presented as mean ± SD, n = 4. * p<0.5, ** p<0.01, *** p<0.001

4.3.7 Apoptosis study

Growth inhibition by leucite and kalsilite glass–ceramic composites at higher concentration raises the question whether it also causes apoptosis of the tumor cells and if so whether it induces cell death. Apoptosis has been determined by monitoring the changes in the cell size and externalization of phosphatidylserine qualitatively in SCC-25 cells [Manna P.P. *et al.* 2013].

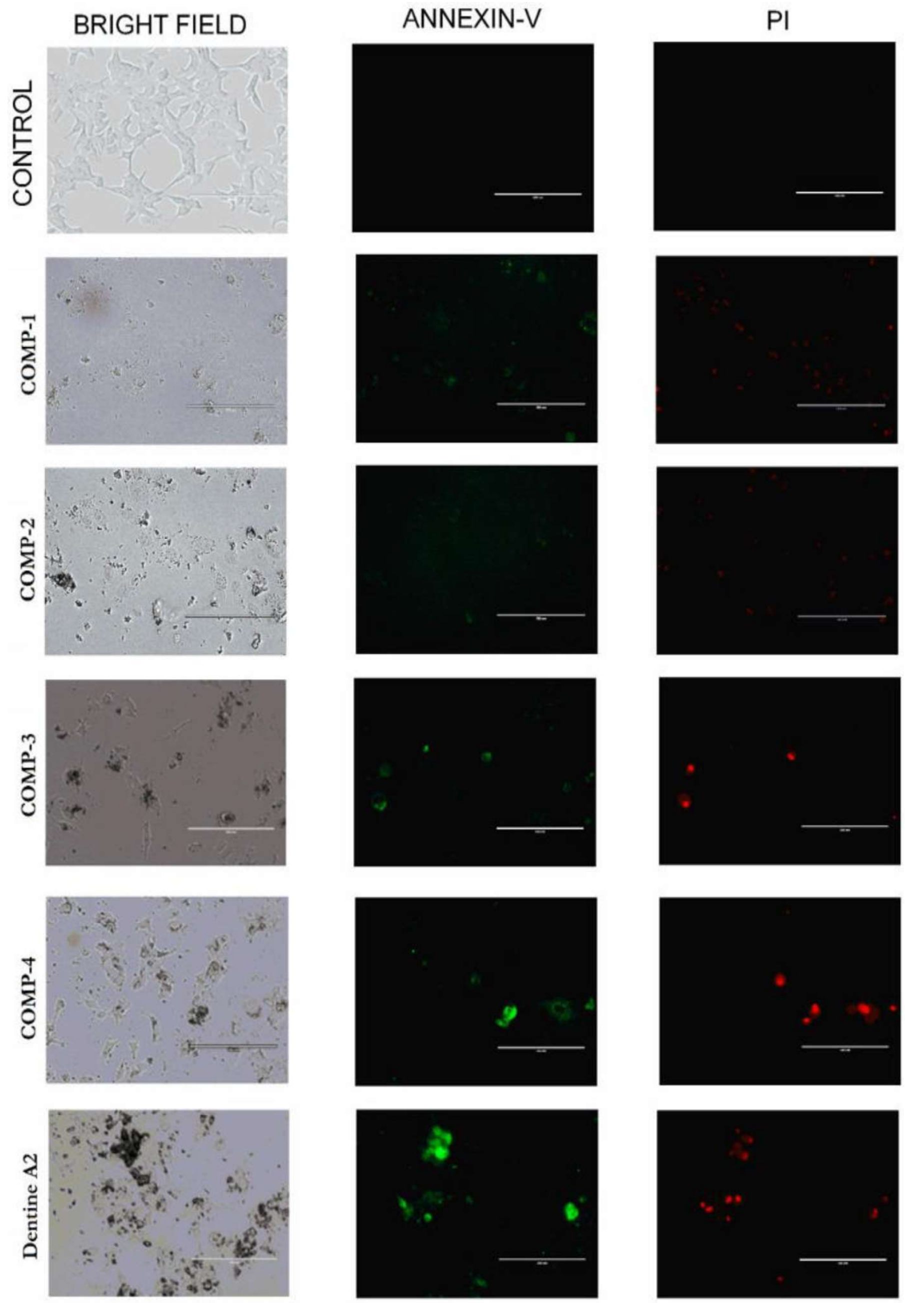

Fig. 4.38 Microscopic analysis of induction of apoptosis SCC-25 cells were given indicated treatment with COMP-1, COMP-2, COMP-3 and COMP-4 glass–ceramic composites materials at a concentration of 50mg/ml in complete RPMI 1640 medium for 8h at 37 ^{o}C. FITC-conjugated Annexin V and Propidium iodide (PI) stained apoptotic cells were visualized under a fluorescence microscope (Nikon Eclipse 80i, Nikon, Japan) with Plan Fluor, 40X, NA 0.75 objective equipped with green and red filters for FITC and PI, respectively. n=3

There is a moderate increase in Annexin V positive cells upon treatment with compositions COMP-3 & COMP-4 (50 mg/ml) and the standard (STD) (Fig. 4.38). The other composite material causes no apoptosis in SCC-25 cells (Fig. 4.38).

4.3.8 Culture of SCC-25 cells on leucite and kalsilite glass–ceramic composites

SCC-25 cells have been cultured on the leucite and kalsilite glass–ceramic composites to demonstrate both the cytocompatibility and biocompatibility of the compounds in the case of clinical application. It has been observed that leucite and kalsilite based glass–ceramic composites are tolerant to the growth of the SCC-25 cells. This is consistent with our results as observed concerning growth inhibition and cytotoxicity (Figs. 4.39-4.43).

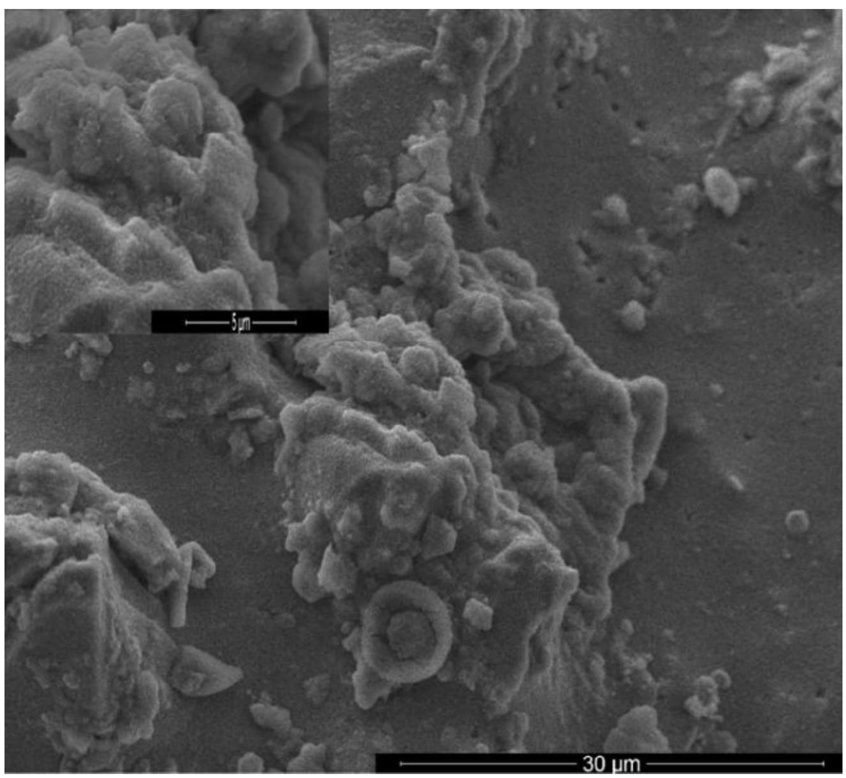

Fig. 4.39 SEM images of the surface of COMP-1showing the proliferation and spreading of SCC-25 cells after 10 days of culture on COMP-1 glass–ceramic composites (image at same magnification and scale bar represent 30μm (inset)

The results also suggest that the prepared composite materials perform better as compared to the standard materials and allow efficient growth of the cells over its surface (Figs. 4.39-4.42).

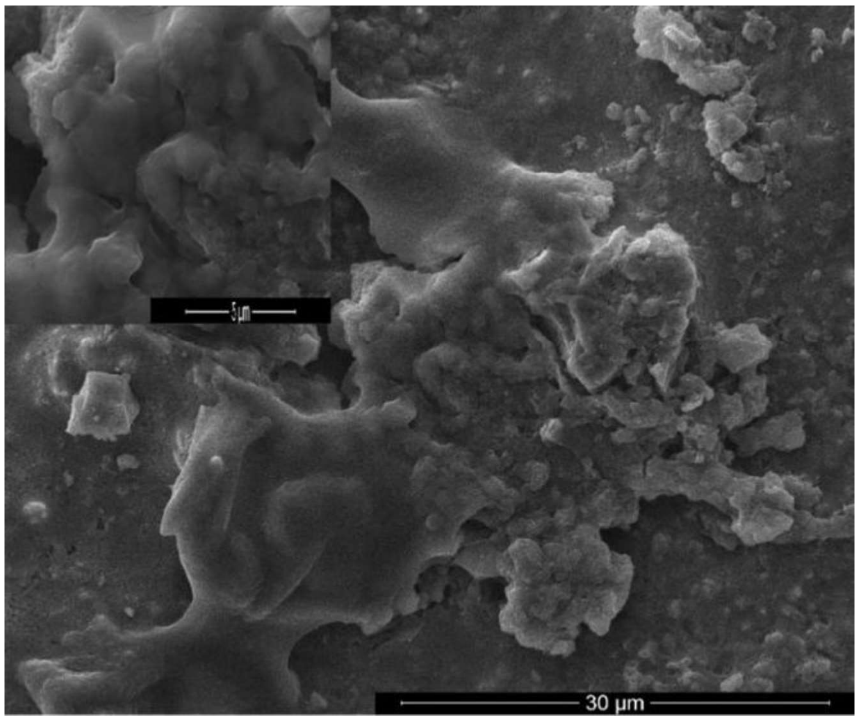

Fig. 4.40 SEM image of the surface of COMP-2 showing the proliferation and spreading of SCC-25 cells after 10 days of culture on COMP-2 (image at same magnification and scale bar represent 30µm (inset)

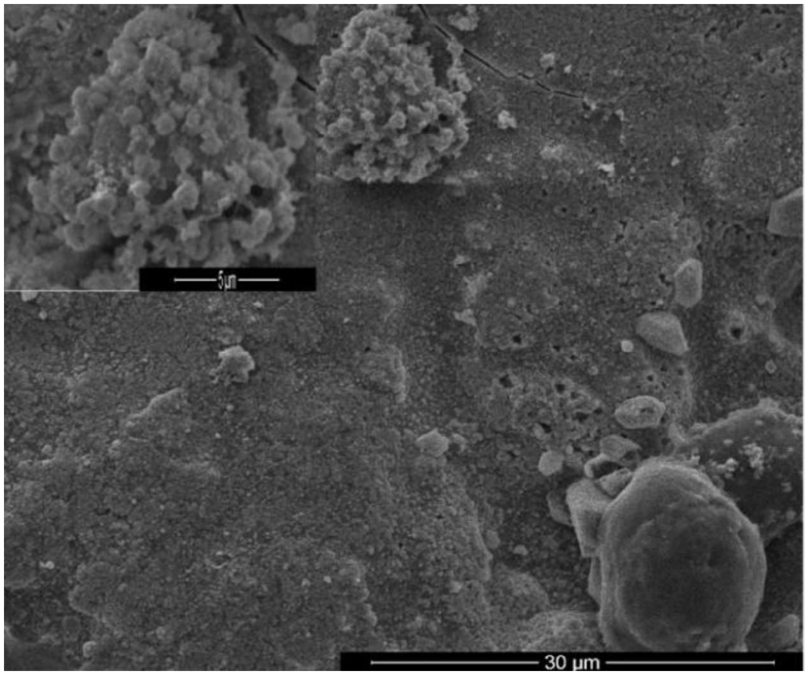

Fig. 4.41 SEM image of the surface of COMP-3 showing the proliferation and spreading of SCC-25 cells after 10 days of culture on COMP-3 (image at same magnification and scale bar represent 30µm (inset)

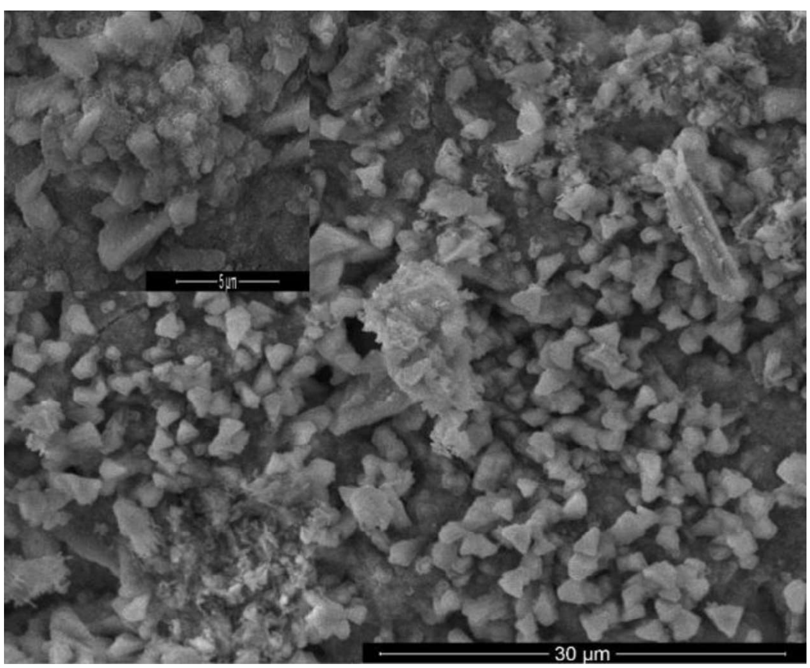

Fig. 4.42 SEM image of the surface of COMP-4 showing the proliferation and spreading of SCC-25 cells after 10 days of culture on COMP-4 (image at same magnification and scale bar represent 30µm (inset)

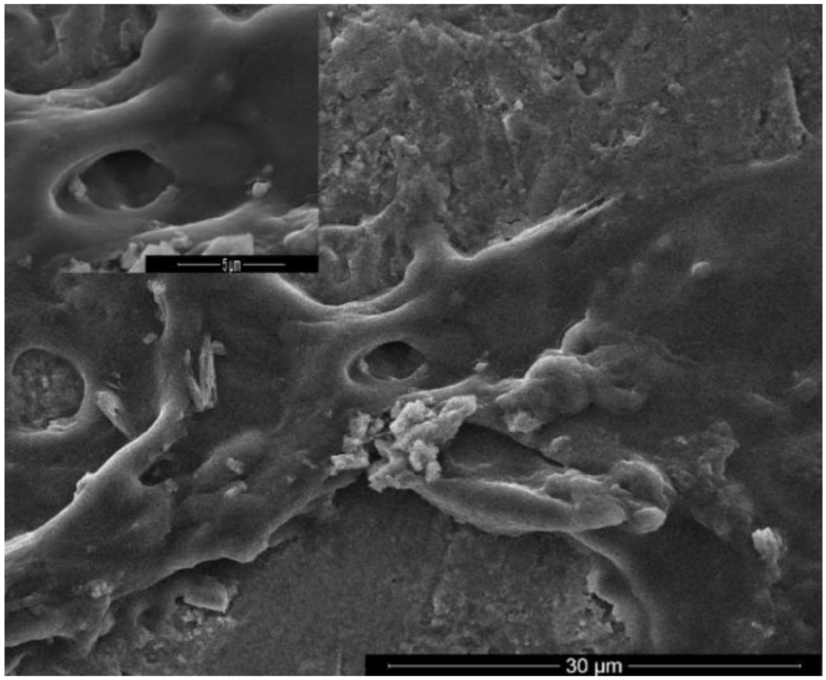

Fig. 4.43 SEM image of the surface of commercial dentine showing the proliferation and spreading of SCC-25 cells after 10 days of culture on dentine (image at same magnification and scale bar represent 30μm (inset)

4.3.9 Summary of the results

Mechanochemically derived leucite and kalsilte based bioactive glass ceramic composites have been prepared successfully for possible dental restorations. All the compositions show similar thermal and mechanical behavior to that of the commercial product. In the present study, the optimum bond has been achieved between the composite and substrate interface layer. The developed leucite and kalsilite bioactive glass ceramic composites applied as a veneer on the surface of commercial dental ceramic substrate generating bioactive coating. The leucite and kalsilite glass–ceramic composites are cytocompatible with negligible effect on cellular proliferation and direct cytotoxicity.

4.4 Effect of Al_2O_3 on leucite based bioactive glass ceramic composite for dental veneering

4.4.1 Phase analysis

Fig. 4.44 exhibits the XRD patterns of the composites before heat treatment. In the composites, leucite has been found to be a major crystalline phase along with alumina phase. The diffraction peaks matched to the JCPDS Card No. 87-1707 and 81-1667. It is seen that the intensity of the peak corresponding to Al_2O_3 phase increases with increasing the alumina content in the matrix. Fig. 4.45 shows the XRD patterns of the composite samples after heat treatment. The diffraction peaks matched to JCPDS Card No. 74-0387 and 81-1667.

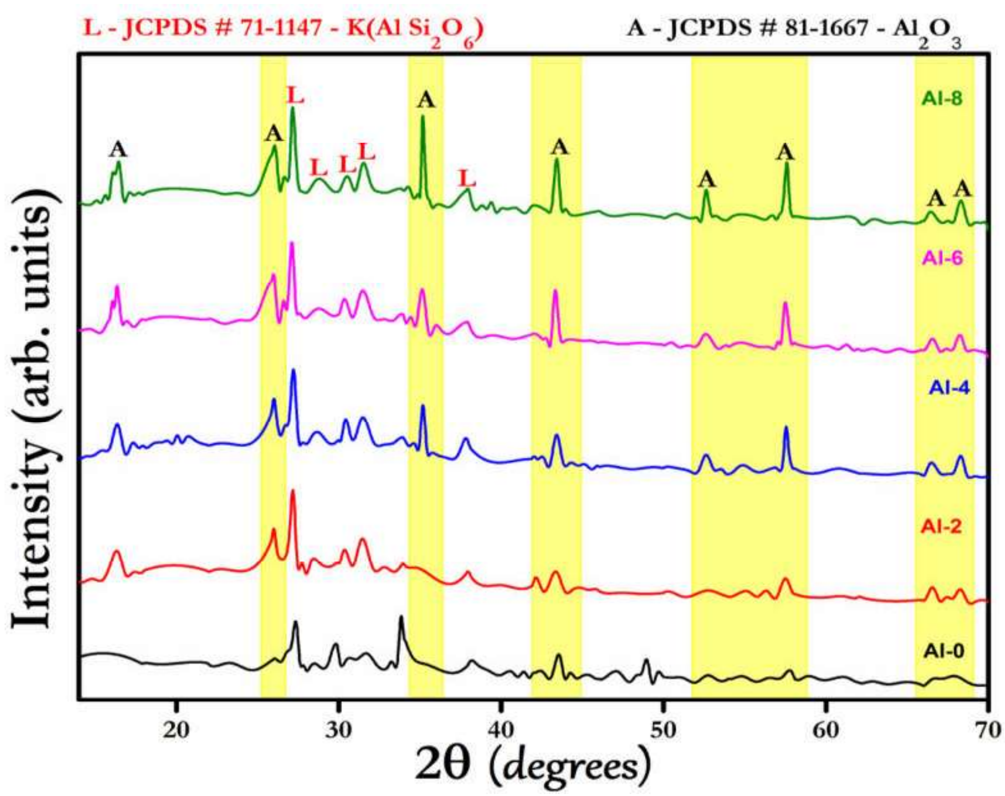

Fig. 4.44 XRD pattern of the composites containing different wt. % of alumina before firing

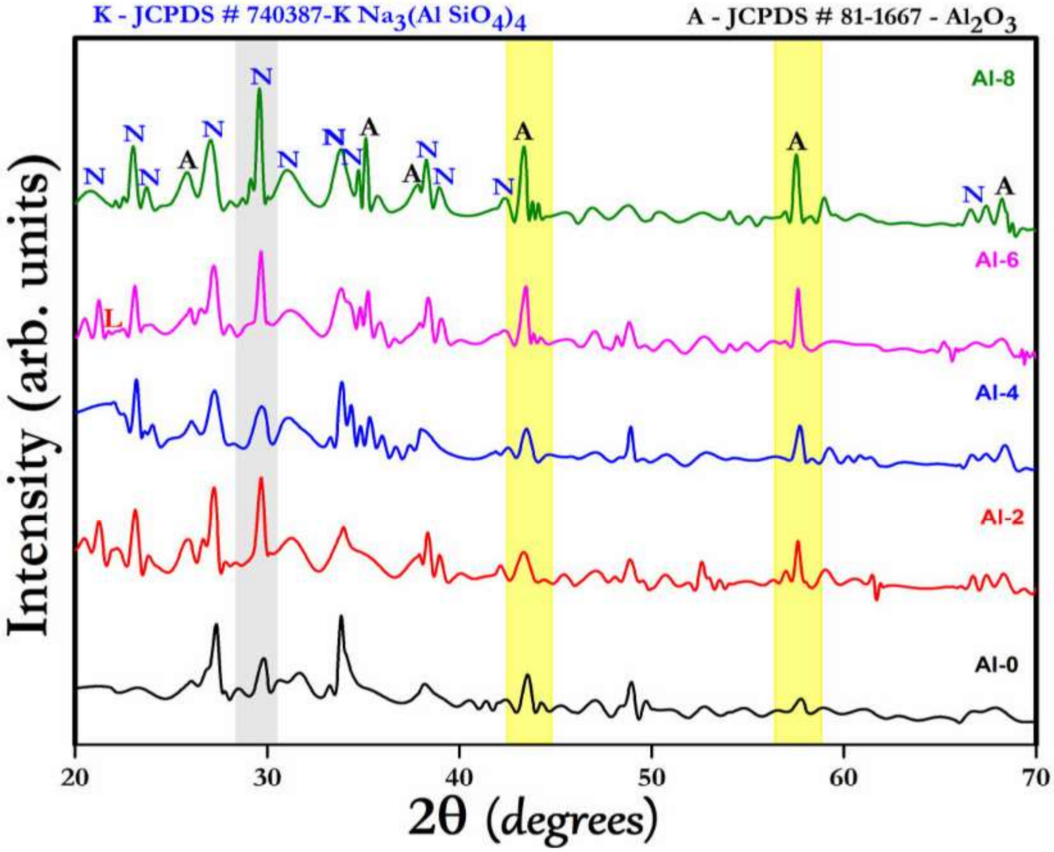

Fig. 4.45 XRD pattern of the composites containing different wt. % of alumina after heat treatment at 960 °C.

It is seen from Fig.4.45 that a major crystalline phase nepheline has formed after firing (at 950 °C) along with some alumina crystalline phase subsequently decreasing the amorphous phase. A second phase nepheline is formed due to the reaction of alumina with the free ions (K^+, Na^+ and Si^{4+}) present in the matrix during heat treatment. Nepheline has the high coefficient of thermal expansion and good mechanical strength which may further increase the mechanical properties of the prepared composites [Hamzawy E.M.A. and El-Meliegy E.A.M. 2008].

4.4.2 Microstructure

Figs. 4.46-4.48 show the surface morphology of Al-0%, Al-4% and Al-8% composites. It is seen that glassy surface reduces slightly with increasing the content of fine alumina in the composites. It is due to the presence of crystalline alumina particles which are distributed homogeneously in the glassy matrix. Micrographs show a very dense morphology with no visible micro-crack on the surface. SEM micrographs along with the EDX spectra of the compositions, Al-0% and Al-8% are shown in Figs. 4.49-4.50. EDX spectra confirm the presence of all the constituent elements (Na, K, Ca, Si, Al, O) in an expected concentration.

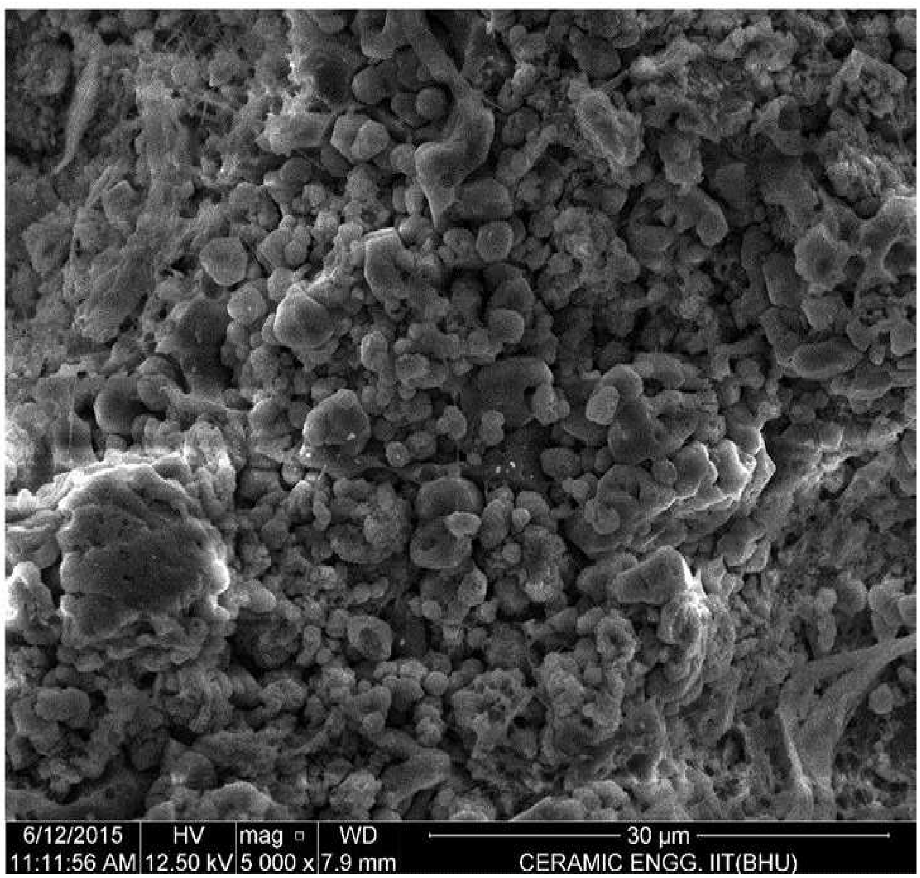

Fig. 4.46 SEM morphology of the composite Al-0 after heat treatment

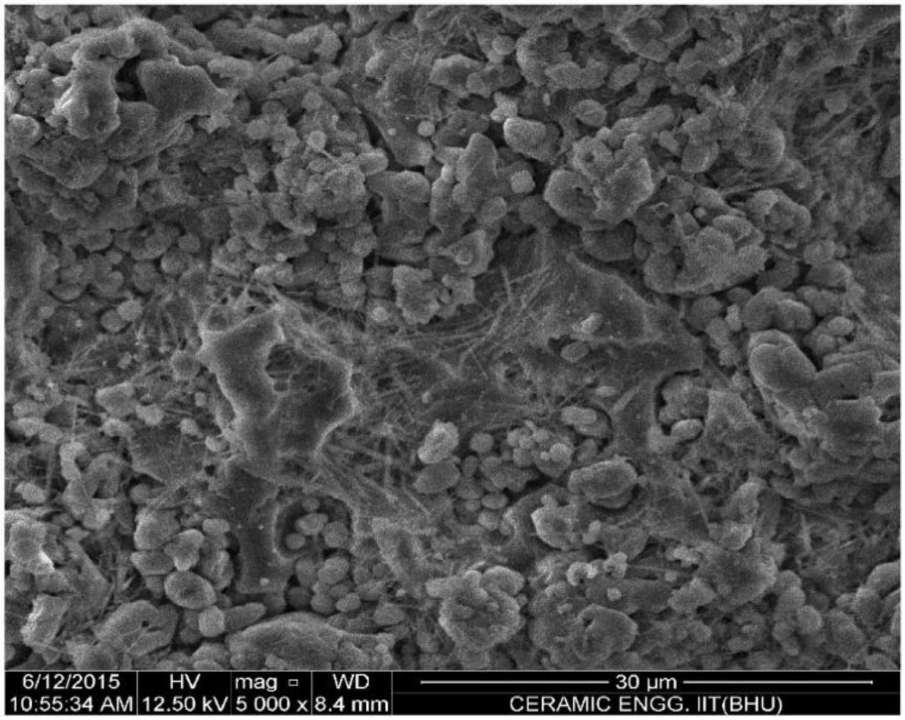

Fig. 4.47 SEM morphology of the composite Al-4 after heat treatment

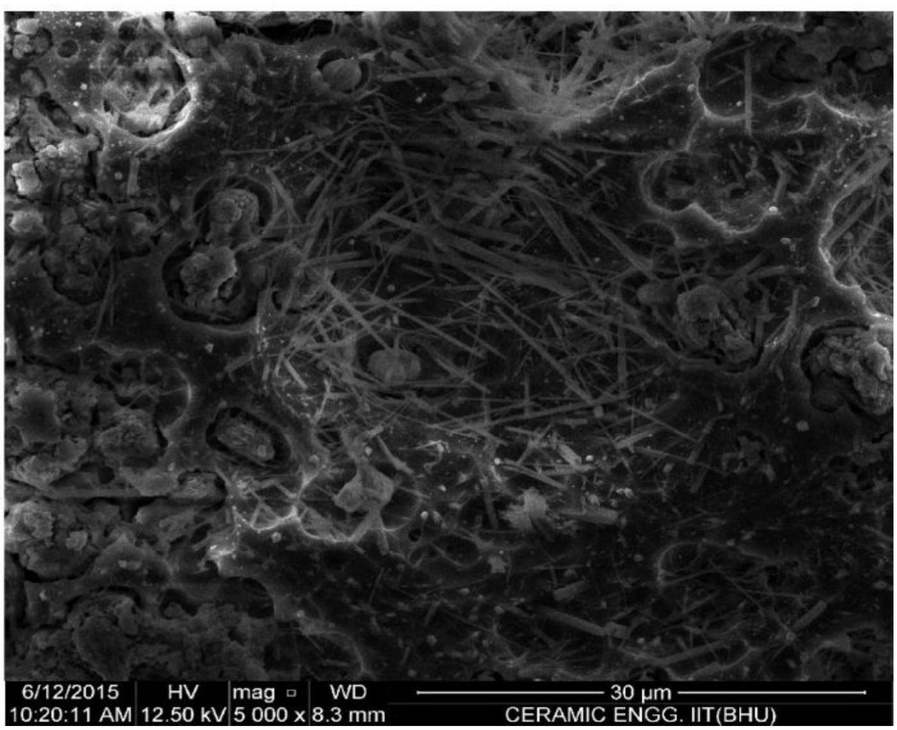

Fig. 4.48 SEM morphology of the composite Al-8 after heat treatment

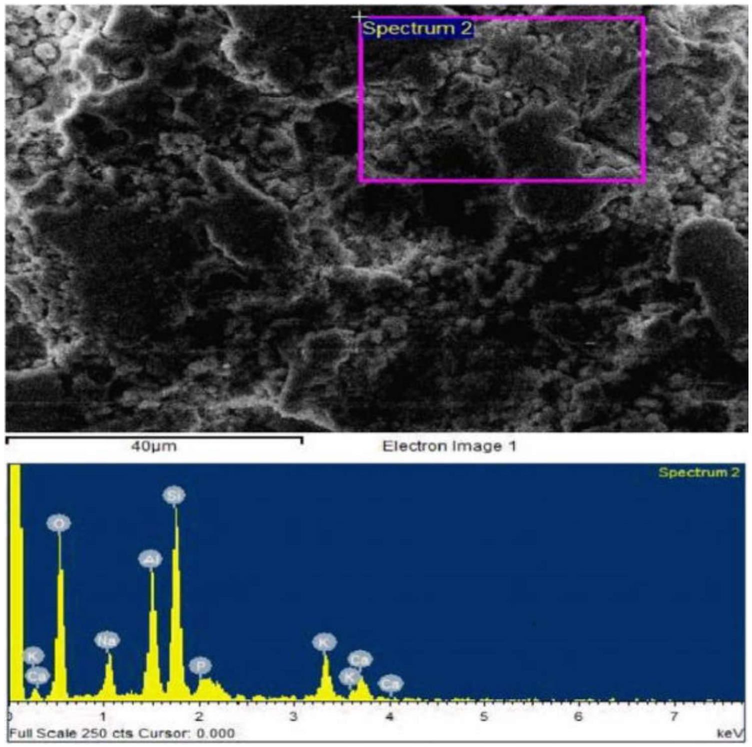

Fig.4.49 SEM and EDS spectrum of the composition Al-0

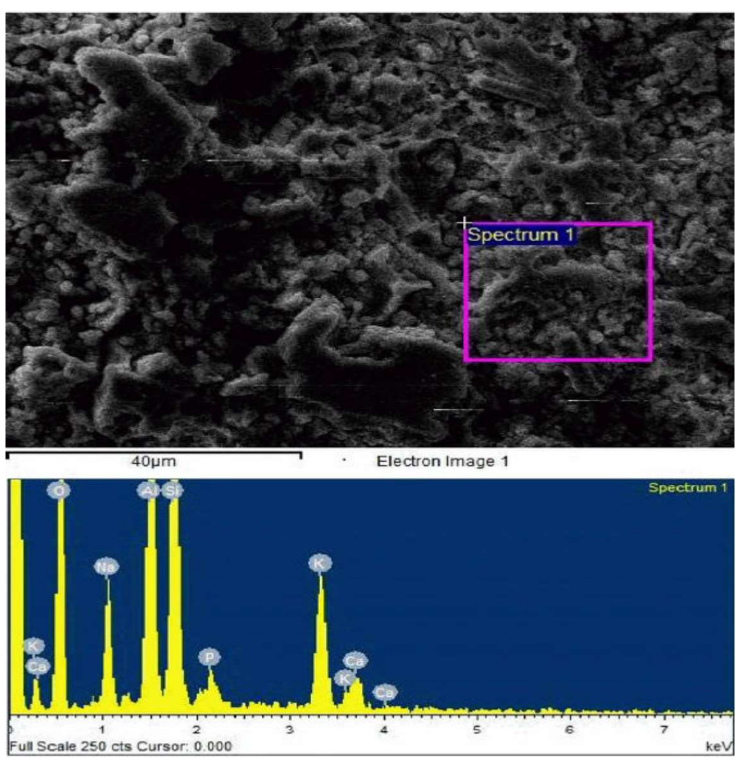

Fig. 4.50 SEM and EDS spectrum of the composition Al-8

4.4.3 Coefficient of thermal expansion (CTE)

Fig. 4.51 shows the CTE curves of the composites along with the commercial dentine (VITA VMK 2M2). It has been observed that the compositions, Al-0, Al-4, Al-8 and VITA dentine have CTE values $14.8\times10^{-6}/°C$, $15.0\times10^{-6}/°C$, $17.8\times10^{-6}/°C$ and $14.5\times10^{-6}/°C$ respectively. CTE of the composites, Al-0 and Al-4 is very close to that of commercial dentin. It is seen from Fig. 4.51 that thermal expansion of the composition Al-8 increases linearly i.e. there is no glass transition. It is due to the high content of alumina present in the matrix. It is found that the addition of fine alumina to the composites increases the CTE of the final mixture.

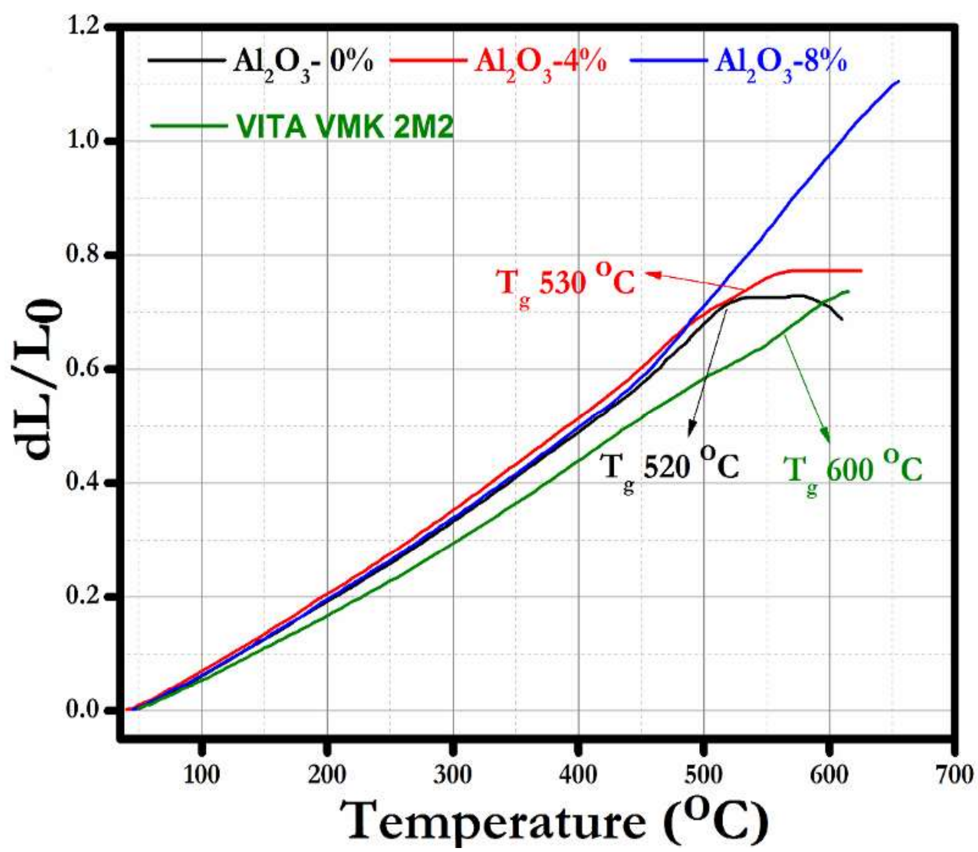

Fig. 4.51 CTE curves of the composites along with commercial dentine (VITA VMK 2M2)

This is due to the presence of nepheline crystalline phase (as seen from XRD patterns in Fig.4.45) which has the high CTE in the range 12.1-16.6×10^{-6}/K [Nan-Chung W. and Min-Hsiung H. 1994]. Khater et al. have also been reported that the formation of nepheline in the glass-ceramic increases the CTE of the matrix [Khater G.A. *et al.* 2013]. These prepared composite materials are, therefore, suitable for PFM as its CTE values are close to that of nickel–chrome alloy (13.9×10^{-6} /°C).

4.4.4 Bulk density (BD) and apparent porosity (AP)

Fig. 4.52 shows the BD and AP of the bioactive glass ceramic composites containing different wt. % of alumina. It is seen from Fig. 4.52 that BD increases (from 1.93 to 2.26 gm/cc) with increasing the alumina content followed by a continuous decrease in the AP.

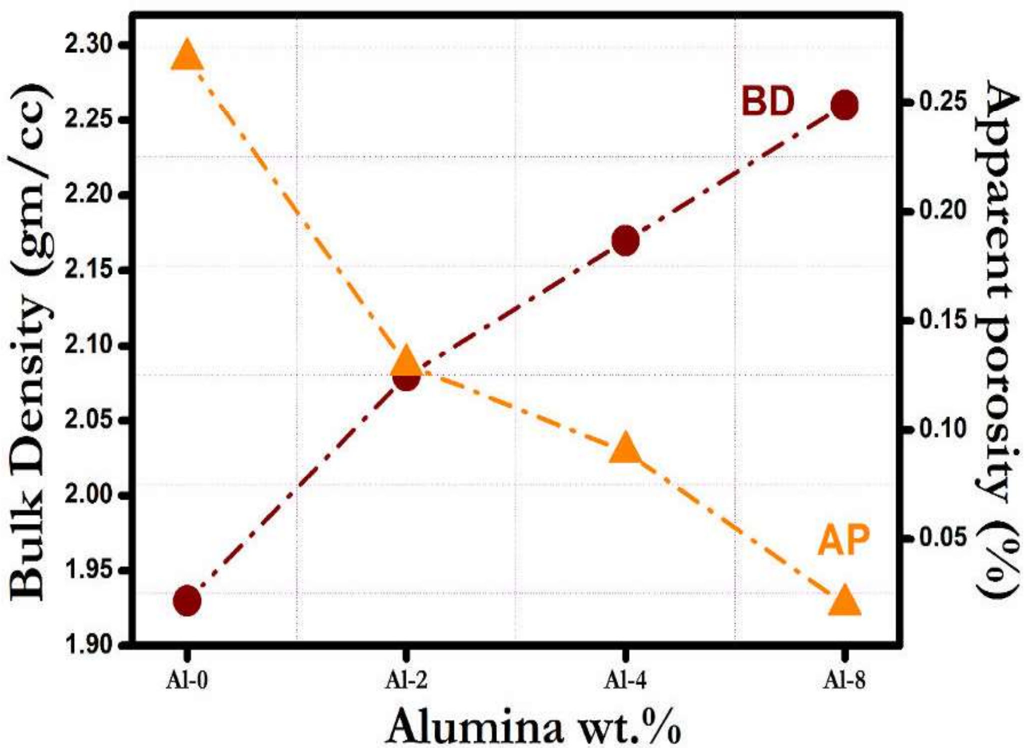

Fig. 4.52 BD and AP of the bioactive glass ceramic composites with different wt. % of alumina

Micro fine alumina particles homogeneously dispersed throughout the glassy matrix, improves the packing density of the composites consequently reduces the apparent porosity.

4.4.5 Flexural strength

Fig. 4.53 shows the flexural strength of the composite and the commercial dentine VITA VMK 2M2. Flexural strength increases with increasing the fine alumina in the matrix. Homogeneous dispersion of fine alumina particles within the glassy matrix leads to enhance the mechanical strength. This is because a crack cannot pass easily through the crystalline alumina particles whereas, in the case of a glassy matrix, it passes easily and hence decreases the mechanical strength.

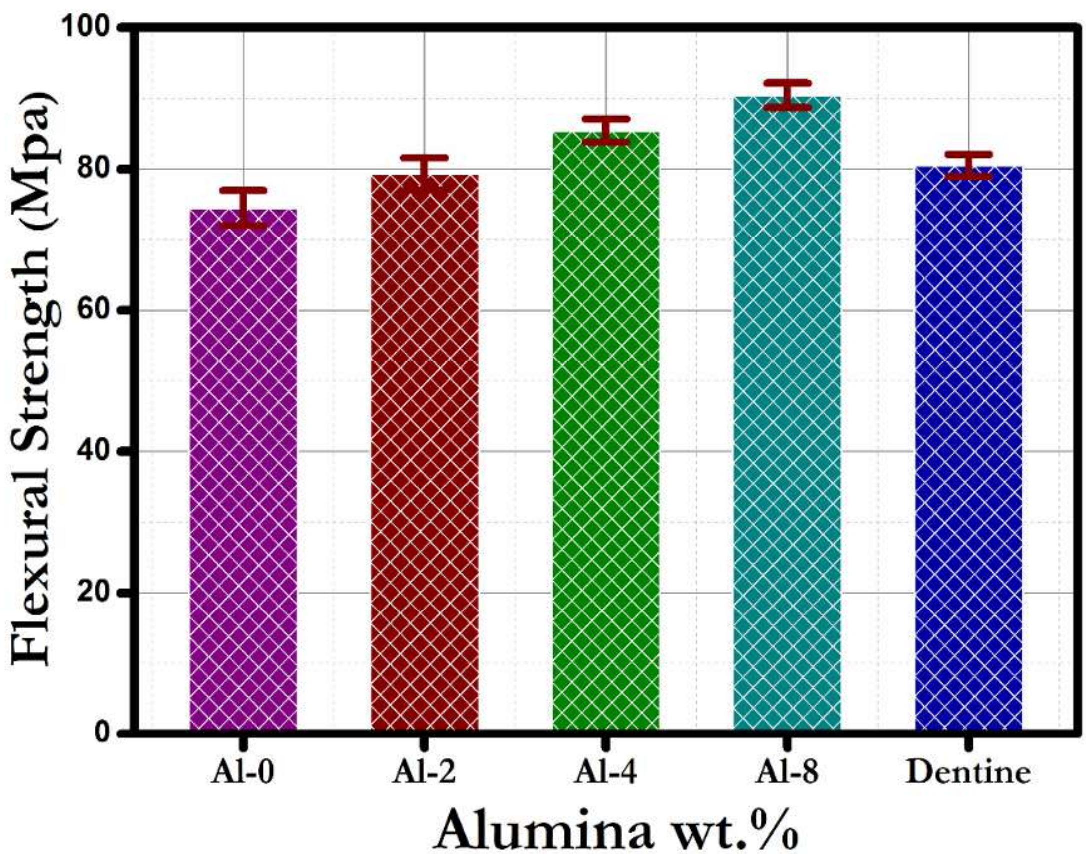

Fig. 4.53 Flexural strength of composites and commercial dentine

This technique has also been used in the dentistry for the development of aluminous porcelains [McCabe F.J. 2008]. Consequently, the synthesized composites show the superior sinterability, low porosity and high flexural strength. The strength of all the alumina added composites is nearly similar to that of the commercial dentine. One of the reasons for enhancement in the flexural strength of the alumina added composites is the formation of crystalline nepheline phase. It has also been reported in the literature that nepheline increases the mechanical strength of the glass-ceramics [Hamzawy E.M.A. and El-Meliegy E.A.M. 2008]. It is, therefore, concluded that fine alumina particles act as a 'crack stoppers' preventing the propagation of a crack throughout the body of the porcelain.

4.4.6 Culture of SCC-25 cells on glass–ceramic composites

Figs. 4.54 (a)-(d) show the surface morphology of the alumina added leucite glass–ceramic composites. SEM morphology reveals the proliferation of SCC-25 cells after 10 days of culture and it covers the whole surface of the sample. The images also show that the cells adhered to all the composites with a flattened and lengthened morphology. Higher numbers of cells are attached on the surface of composites Al-2 and Al-4. This is consistent with our results as observed concerning to growth inhibition and cytotoxicity [Fig.4.54 (b) & (c)]. These results also suggest that the prepared composite material allows the efficient growth of the cells over its surface (Fig. 4.54).

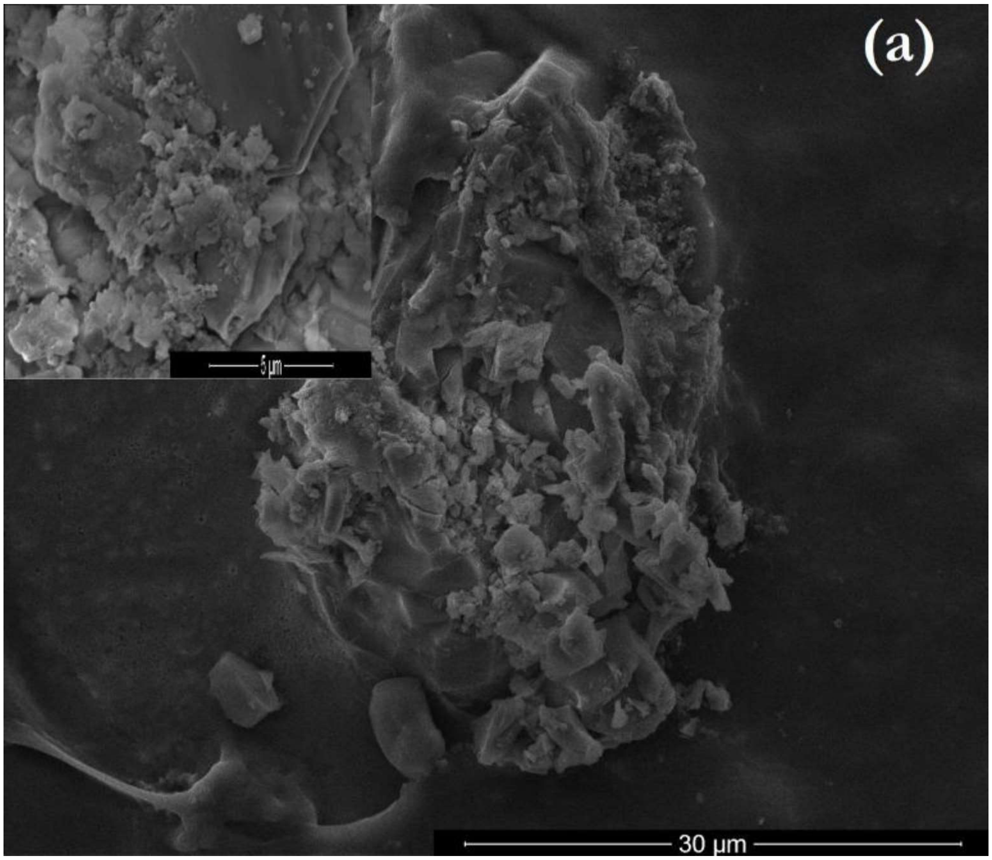

Fig. 4.54 (a) Surface morphology of the sample Al-0 showing the proliferation and spreading of SCC-25 cells after 10 days of culture

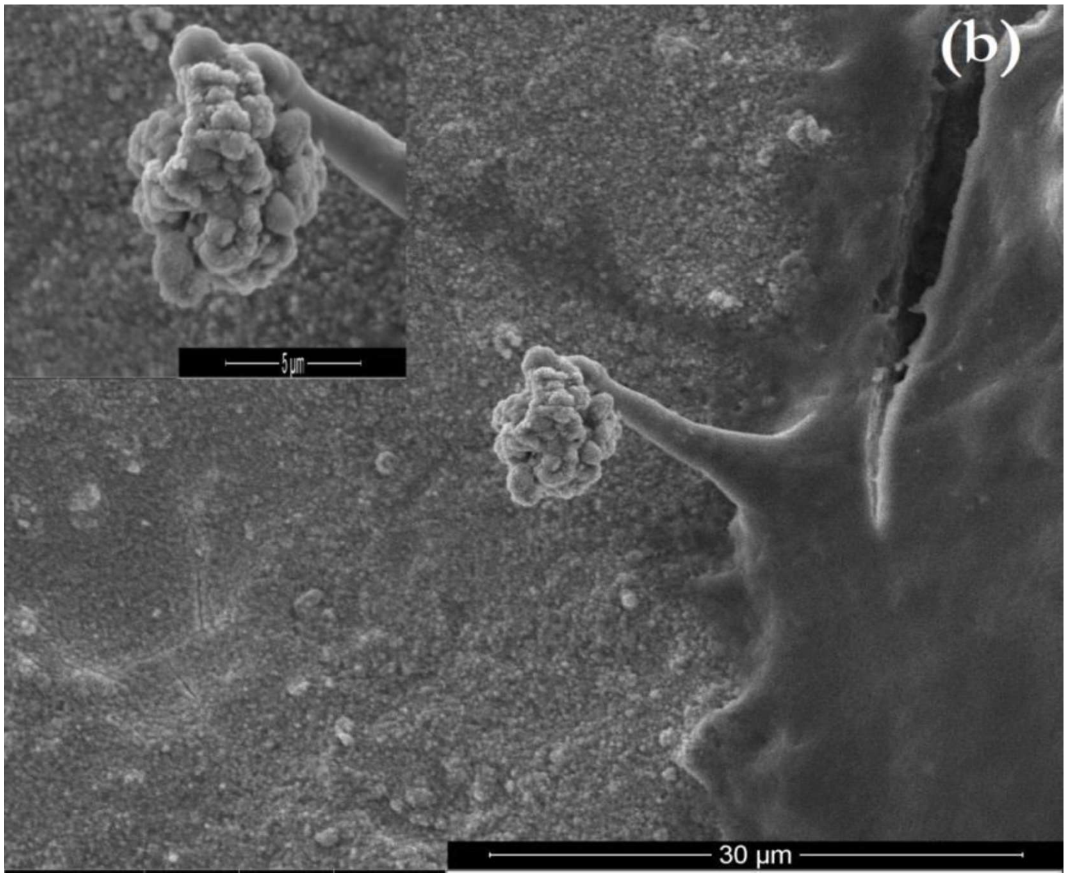

Fig. 4.54 (b) Surface morphology of the sample Al-2 showing the proliferation and spreading of SCC-25 cells after 10 days of culture

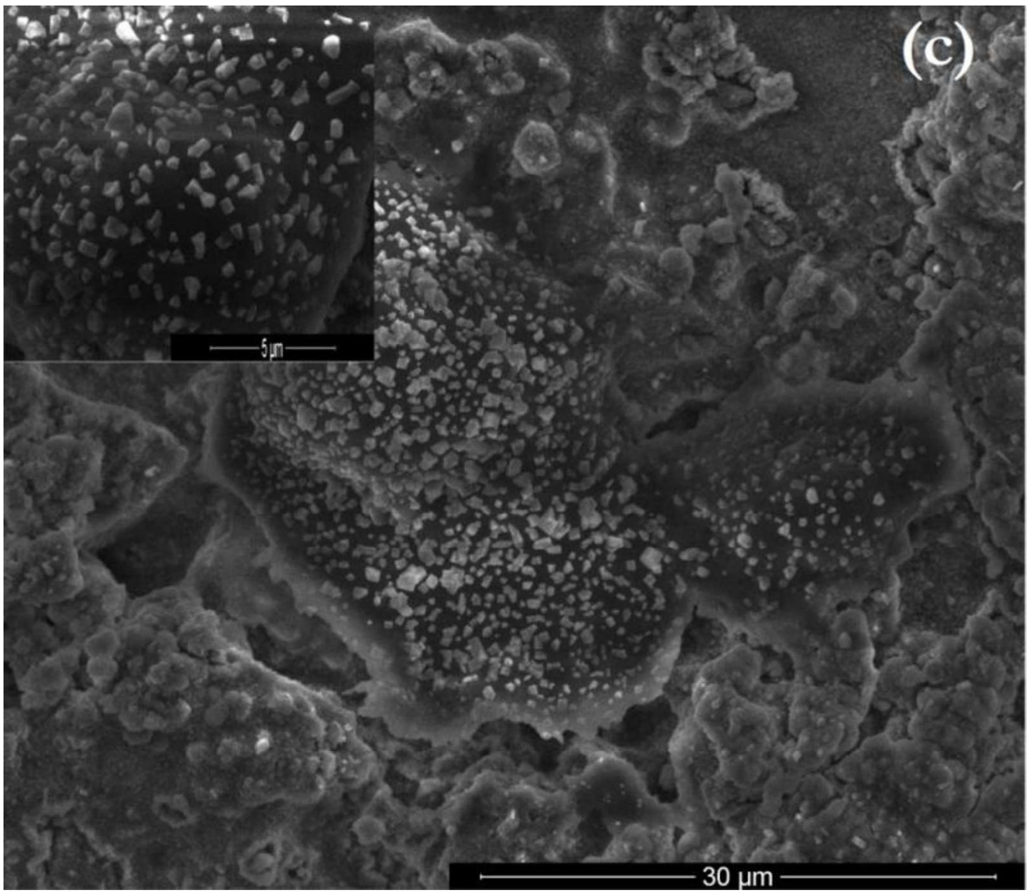

Fig. 4.54 (c) Surface morphology of the sample Al-4 showing the proliferation and spreading of SCC-25 cells after 10 days of culture

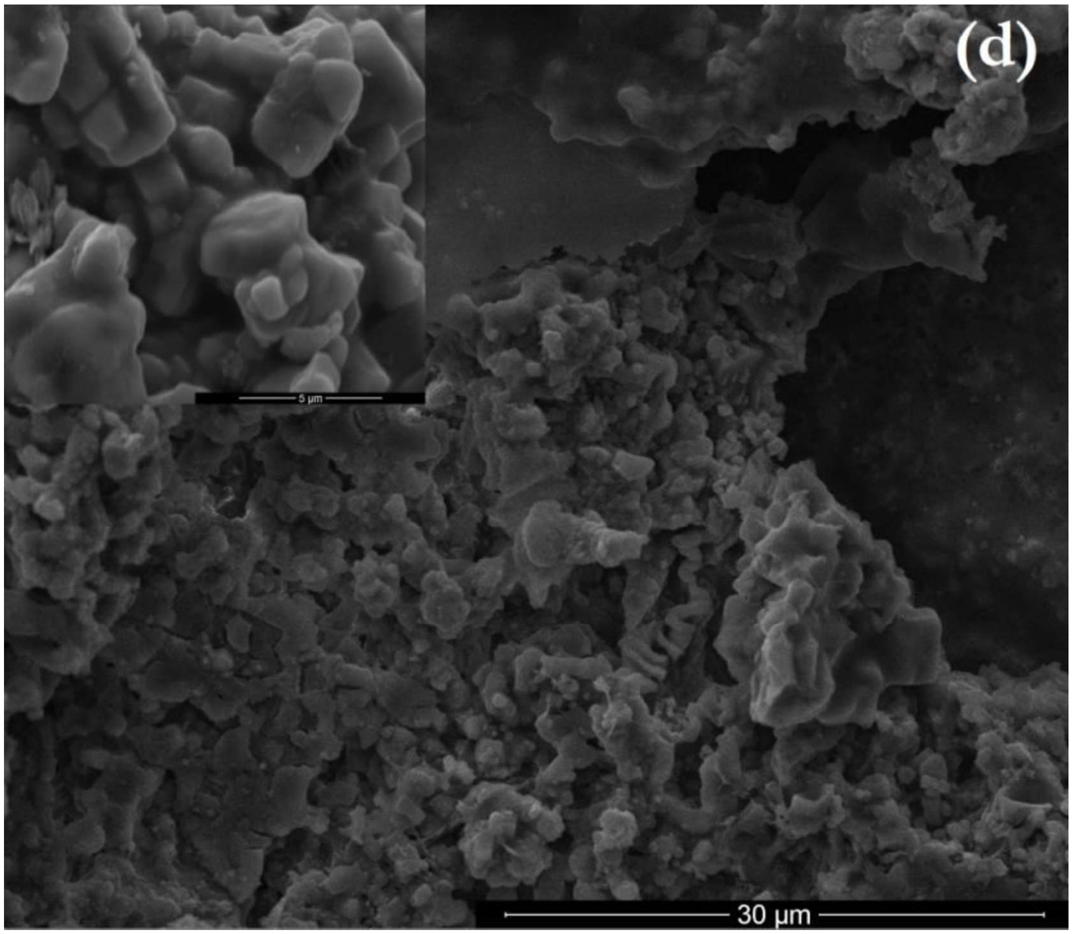

Fig. 4.54 (d) Surface morphology of the sample Al-8 showing the proliferation and spreading of SCC-25 cells after 10 days of culture

4.4.7 Summary of the results

This study has shown the successful investigation of alumina added leucite glass ceramic composites for possible applications in the dental restorations. The addition of alumina to the glass ceramic composites results in the formation of nepheline crystalline phase. This leads to enhance the CTE and flexural strength of the samples. Alumina added leucite glass ceramic composites show high flexural strength (80-90 MPa) than that of the leucite based glass ceramic composites (74-78 MPa) and the commercial dentine (79 MPa). A uniform attachment of SSC-25 cells after 10 days of culture on the surface of the composites has been observed. It confirms that the addition of alumina to the leucite glass ceramic composite is a successful approach to improving its mechanical and biological properties.